NASA/TM—2006-214023

Slow Crack Growth and Fracture Toughness of Sapphire for the International Space Station Fluids and Combustion Facility

Jonathan A. Salem
Glenn Research Center, Cleveland, Ohio

January 2006

The NASA STI Program Office . . . in Profile

Since its founding, NASA has been dedicated to the advancement of aeronautics and space science. The NASA Scientific and Technical Information (STI) Program Office plays a key part in helping NASA maintain this important role.

The NASA STI Program Office is operated by Langley Research Center, the Lead Center for NASA's scientific and technical information. The NASA STI Program Office provides access to the NASA STI Database, the largest collection of aeronautical and space science STI in the world. The Program Office is also NASA's institutional mechanism for disseminating the results of its research and development activities. These results are published by NASA in the NASA STI Report Series, which includes the following report types:

- TECHNICAL PUBLICATION. Reports of completed research or a major significant phase of research that present the results of NASA programs and include extensive data or theoretical analysis. Includes compilations of significant scientific and technical data and information deemed to be of continuing reference value. NASA's counterpart of peer-reviewed formal professional papers but has less stringent limitations on manuscript length and extent of graphic presentations.

- TECHNICAL MEMORANDUM. Scientific and technical findings that are preliminary or of specialized interest, e.g., quick release reports, working papers, and bibliographies that contain minimal annotation. Does not contain extensive analysis.

- CONTRACTOR REPORT. Scientific and technical findings by NASA-sponsored contractors and grantees.

- CONFERENCE PUBLICATION. Collected papers from scientific and technical conferences, symposia, seminars, or other meetings sponsored or cosponsored by NASA.

- SPECIAL PUBLICATION. Scientific, technical, or historical information from NASA programs, projects, and missions, often concerned with subjects having substantial public interest.

- TECHNICAL TRANSLATION. English-language translations of foreign scientific and technical material pertinent to NASA's mission.

Specialized services that complement the STI Program Office's diverse offerings include creating custom thesauri, building customized databases, organizing and publishing research results . . . even providing videos.

For more information about the NASA STI Program Office, see the following:

- Access the NASA STI Program Home Page at ***http://www.sti.nasa.gov***

- E-mail your question via the Internet to help@sti.nasa.gov

- Fax your question to the NASA Access Help Desk at 301–621–0134

- Telephone the NASA Access Help Desk at 301–621–0390

- Write to:
  NASA Access Help Desk
  NASA Center for AeroSpace Information
  7121 Standard Drive
  Hanover, MD 21076

NASA/TM—2006-214023

Slow Crack Growth and Fracture Toughness of Sapphire for the International Space Station Fluids and Combustion Facility

Jonathan A. Salem
Glenn Research Center, Cleveland, Ohio

National Aeronautics and
Space Administration

Glenn Research Center

January 2006

Acknowledgments

Thanks to Robert Polvani and David Black of National Institute of Standards and Technology (NIST), Manufacturing Metrology Division, Gaithersburg, MD for the X-ray topography. Thanks to Shelly Wiederhorn of NIST for many useful discussions. Thanks to William Scott of the University of Washington for many useful discussions and for etching work. Thanks to R.O. Ritchie of the University of California, Berkeley for supplying a fractured *m*-plane test specimen. The Microgravity Sciences Fluids and Combustion Facility funded the work.

Available from

NASA Center for Aerospace Information
7121 Standard Drive
Hanover, MD 21076

National Technical Information Service
5285 Port Royal Road
Springfield, VA 22100

Available electronically at http://gltrs.grc.nasa.gov

Slow Crack Growth and Fracture Toughness of Sapphire for the International Space Station Fluids and Combustion Facility

Jonathan A. Salem
National Aeronautics and Space Administration
Glenn Research Center
Cleveland, Ohio 44135

Summary

The fracture toughness, inert flexural strength, and slow crack growth parameters of the *r*- and *a*-planes of sapphire grown by the Heat Exchange Method were measured to qualify the sapphire for structural use in the International Space Station. The fracture toughness in dry nitrogen, K_{Ipb}, was 2.31±0.12 MPa√m and 2.47±0.15 MPa√m for the *a*- and *r*-planes, respectively. Fracture toughness measured in water via the operational procedure in ASTM C1421 was significantly lower, K_{Ivb} = 1.95±0.03 MPa√m, 1.94±0.07 and 1.77±0.13 MPa√m for the *a*- , *m*- and *r*-planes, respectively. The mean inert flexural strength in dry nitrogen was 1085±127 MPa for the *r*-plane and 1255±547 MPa for the *a*-plane. The power law slow crack growth exponent for testing in water was $n = 21\pm4$ for the *r*-plane and $n \geq 31$ for the *a*-plane. The power law slow crack growth coefficient was $A = 2.81\times10^{-14}$ m/s·(MPa√m)$^{-n}$ for the *r*-plane and $A \cong 2.06\times10^{-15}$ m/s·(MPa√m)$^{-n}$ for the *a*-plane. The *r*- and *a*-planes of sapphire are relatively susceptible to stress corrosion induced slow crack growth in water. However, failure occurs by competing modes of slow crack growth at long failure times and twinning for short failure time and inert environments. Slow crack growth testing needs to be performed at low failure stress levels and long failure times so that twinning does not affect the results.

Some difficulty was encountered in measuring the slow crack growth parameters for the *a*-plane due to a "short" finish (i.e., insufficient material removal for elimination of the damage generated in the early grinding stages). A consistent preparation method that increases the Weibull modulus of sapphire test specimens and components is needed. This would impart higher component reliability, even if higher Weibull modulus is gained at the sacrifice of absolute strength of the component. The current specification frequently used for the preparation of sapphire test specimens and components (e.g., a "60/40" scratch-dig finish) is inadequate to avoid a "short" finish.

1. Introduction

The U.S. "Destiny" laboratory module resides within the International Space Station and contains six science facilities or "racks." One of these facilities is the Fluids and Combustion Facility (FCF), which will be used to study combustion and fluids processes in microgravity. Within this facility is the Combustion Integrated Rack (CIR). This rack consists of a combustion chamber circumferentially surrounded by diagnostics, which image the interior of the chamber through eight viewing "windows" shown in Figure 1. Previously, such windows were made from quartz, however, due to its superior optical properties in certain infrared ranges, sapphire is being considered for the windows.

Sapphire fails from a combination of slow crack growth and twinning, and the interaction between the mechanisms is unknown. The dominant mechanism is likely dependent on the temperature, environment, relative stress level and surface finish. Twinning can be induced with compression or tension, and thus all surfaces of test specimens and components need to be polished adequately. The chamber and windows are required to tolerate 90 percent RH (relative humidity) during storage and transportation, and 75 percent RH atmosphere in the International Space Station. The reported properties of sapphire vary substantially

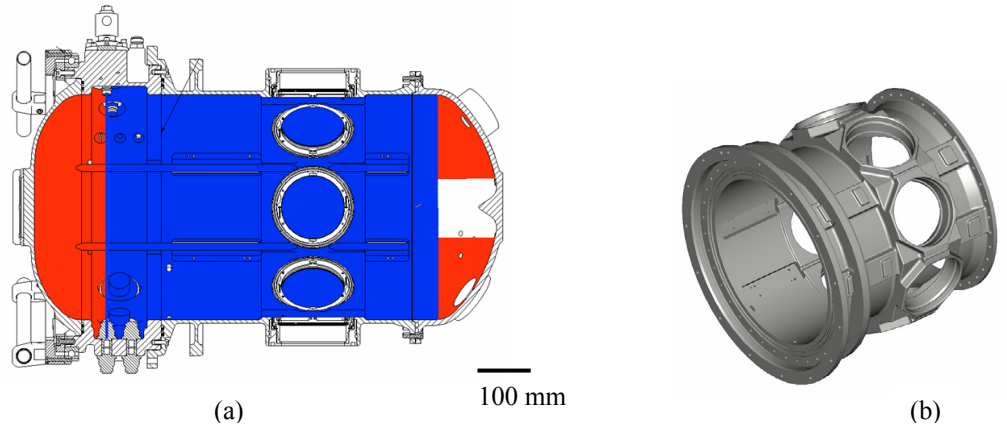

Figure 1.—(a) Cross section of Combustion Integrated Rack chamber assembly and (b) the aluminum window chamber.

for the *r*-plane. Because the application requires highly polished windows to be exposed to low stresses in low temperature, high humidity air, the slow crack growth (SCG) parameters and fracture toughness of the candidate sapphire were measured in water on the *a*- and *r*-planes.

2. Experimental Procedure

2.1 Material

Flexure specimens were ground from sapphire grown by the heat exchange method (HEM)[1] and mechanically diamond polished[2] on the tensile face and sides to a 60/40 scratch dig specification (Ref. 1) by using a random circular motion in order to provide an optical quality surface. The compressive face of the test specimens was left with a ~320 ground finish. Several sets of specimens were made with *a*-, *m*-, or *r*-plane cross sections. For the test specimens with an *r*-plane cross section, the sides corresponded to the *a*-plane. For the specimens with *a*- and *m*-plane cross sections, the tensile surface corresponded to the *c*-plane. These orientations will be referred to as "*a*-plane," "*m*-plane," and "*r*-plane," respectively, as shown in Figure 2. The specimens were oriented within ±2° of the plane specified. During test specimen preparation, the manufacturer requested that some of the test specimen bevels be increased to 0.250 mm from the 0.125 mm specified because difficulty was encountered in eliminating chips from the bevels. The request was approved and the test results have been corrected for the small change (~2.9 percent) in the stress state.

2.2 Elastic Properties

The elastic moduli of some of the flexural specimens were measured by using the impulse excitation technique (Ref. 2). Test specimens were supported at the nodal points with foam strips and the specimen impacted lightly. The resultant impact induced a flexural vibration that was detected with a microphone and automatically recorded with an electronic circuit. The elastic moduli were then calculated from the specimen geometry and measured resonant frequency assuming a Poisson's ratio of 0.26, which corresponds to that of polycrystalline alumina. The elastic constants of Teft (Ref. 3) indicate that Poisson's ratio for the *c*-plane in standard orientation is $\nu = -S_{12}/S_{11} = 0.30$. The elastic moduli in the *a*-, *m*- and *r*-directions were 430±5, 426±4 and 345±2 GPa respectively, in good agreement with the data of Teft (Ref. 3). The individual results are summarized in Table A1 of the appendix.

[1]Crystal Systems, Salem, MA.
[2]Insaco, Quakertown, PA.

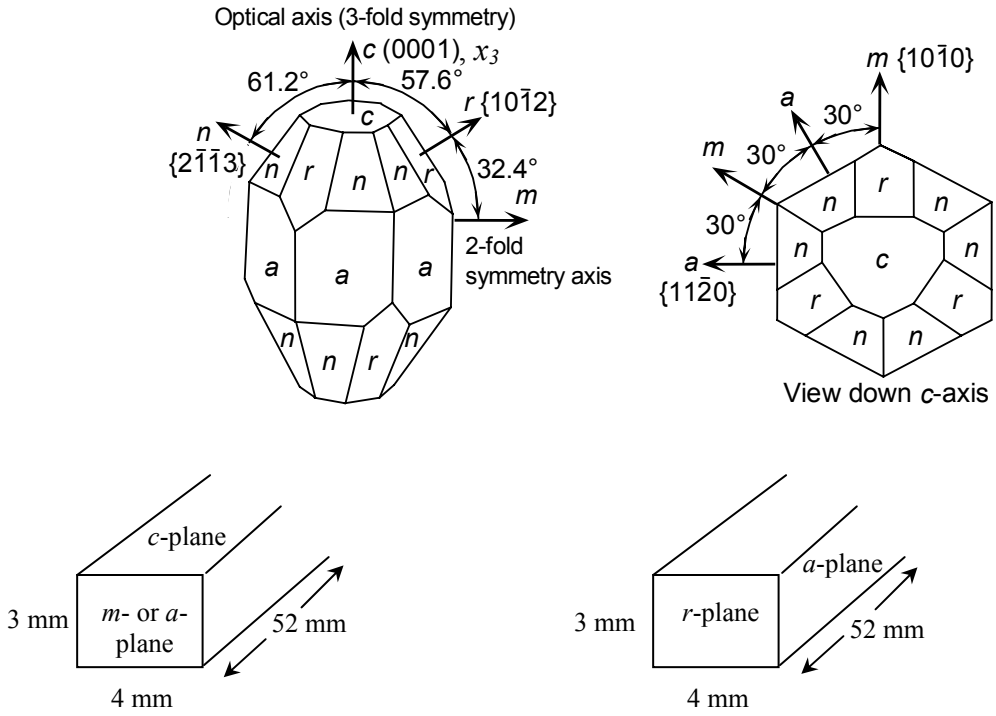

Figure 2.—Test specimen orientation and sapphire crystal showing mineralogical and Miller index notation. The *c*-axis is a 3-fold symmetry axis, but sapphire is indexed as a hexagonal unit cell with $c/a = 2.730$.

2.3 Hardness

The hardness of the *c*-plane was measured by using Knoop and Vickers indentation. For Knoop hardness testing, a load of 0.1 kg was applied for 15s. Occasionally, cracking from the indentation corners occurred and such results were not used in calculations. The measured hardness was HK0.1/15 = 19.6±1.3 GPa. Knoop testing was also attempted at 0.5 kg, however, large lateral cracks formed, making measurements difficult. For Vickers hardness testing, loads of 0.1 and 0.5 kg were applied. The resulting hardness was HV0.1/15 =20.6±1.2 GPa and HV0.5/15 =19.6±1.3 GPa, respectively. Little or no cracking was evident from the indentation corners for 0.1 kg. However for 0.5 kg, significant cracking occurred.

In addition to testing on the *c*-plane, tests were conducted on the *a*- and *m*-planes. Vickers indentation on planes other than the *c*-plane resulted in severely cracked or spherically shaped indentations. The results are summarized in Table A2 of the appendix.

2.4 Fracture Toughness

The fracture toughness of the *a*-, *m*-, and *r*-planes was measured in accordance with standardized procedures (Ref. 4) by using the PB (single-edged-precracked-beam) and VB (chevron-notch beam) methods. Initially, the machining vendor had difficulty grinding chevron notches within the required tolerances due to the high hardness of sapphire. Thus, several sets of PB and VB tests were performed. Witness tests using α SiC were run before each series of tests and gave virtually identical results that compare very well with data from this and other laboratories for the same batch of material (Ref. 5). Water does not wet notches in sapphire well, and thus the test specimens and fixture were submerged in water for 10 to 20 min. prior to load initiation.

2.5 Non-Destructive Inspections

All of the strength and slow crack growth test specimen bevels were checked for severe chips by carefully running a thumbnail along the bevel. This simple procedure identified five *r*-plane and seven *a*-plane specimens with severe chips. These specimens were used for fracture toughness testing rather than strength testing. The majority of *r*-plane specimen bevels were also inspected by optical microscopy, and the gage sections and bevels of six of the *a*-plane specimen were optically inspected in detail at NIST (Ref. 6). In addition to the "thumbnail" and optical inspections, three *r*-plane and 33 *a*-plane specimens were viewed using X-ray topography at Brookhaven National Laboratory (Ref. 6).

2.6 Slow Crack Growth and Inert Strength Testing

The SCG (slow crack growth) behavior of the sapphire was characterized by using the constant stress rate ("dynamic fatigue") method in accordance with ASTM C 1368 (Ref. 7). Testing was conducted by using four-point flexure with 20 mm load and 40 mm support spans in distilled, deionized water at stress rates ranging from 0.002 to 2 MPa/s for the *r*-plane test specimens and 0.002 to 23 MPa/s for the *a*-plane test specimens. An electro-mechanical test system with load control capability was employed.[3] A sheet of 0.125 mm thick graphite was placed between the rollers and the compressive face of the test specimens (Ref. 8). In addition, the compressive face and one-half of the sides of the test specimens were covered with cellophane tape to aid fractography. The stress rates were intentionally kept much smaller than typically used in strength (~35 MPa/s) and SCG testing in order to minimize averaging of the three regions of the SCG curve (Ref. 9).

The inert strength was determined by testing specimens in high purity (99.98 percent) dry nitrogen after vacuum drying for more than 4 hours. The test fixtures and equipment were identical to that used for the SCG measurements. In addition to using the inert environment, the stress rate was increased to 300 MPa/s in order to minimize any stable crack extension associated with region III of the SCG curve.

3. Analyses

3.1 Slow Crack Growth Parameter Analysis

The stress rate as a function of load rate for four-point flexure is

$$\dot{\sigma} = \frac{3}{2}\frac{\dot{P}(S_o - S_i)}{bw^2} \tag{1}$$

where $\dot{P}$ is the load rate, b is the specimen width, w is the height and S_o and S_i are the outer and inner spans. The use of different stress rates provides time for the flaws in the material to grow to different sizes via stress corrosion prior to specimen failure, thereby indicating the sensitivity of the material to the test environment. For ceramics and glasses, the slow crack growth rate under Mode *I* loading above the SCG limit is generally expressed by the power-law relations (Ref. 10)

$$v = \frac{da}{dt} = A^* \left[\frac{K_I}{K_{IC}}\right]^n = AK_I^n \tag{2}$$

where *v, a* and *t* are crack velocity, crack size and time, respectively. The material/environment dependent SCG parameters are *A or A** and *n.* The values K_I and K_{IC} are, respectively, the applied Mode *I* stress

[3]Instron model 8562, Instron Corp., Canton MA.

intensity factor and the critical stress intensity factor or fracture toughness of the material. For SCG testing that employs a constant load or stress rate, the corresponding SCG fracture strength, σ_f, can be expressed as a function of stress rate, $\dot{\sigma}$, as follows (Ref. 10)

$$\sigma_f = \left[B(n+1)\sigma_i^{n-2}\dot{\sigma}\right]^{1/n+1} \tag{3}$$

where σ_i is the inert strength, and B is a parameter associated with A or A^*, n, fracture toughness, crack geometry and loading configuration. The parameter n is determined from the slope of log σ_f plotted as a function of log $\dot{\sigma}$ with Equation (3) written as

$$\log \sigma_f = \frac{1}{n+1}\log \dot{\sigma} + \log D \tag{4}$$

where

$$\log D = \frac{1}{n+1}\log\left[B(n+1)\sigma_i^{n-2}\right] \tag{5}$$

Once the slope α and intercept β of Equation (4) are estimated via linear regression, the parameters n, D, B and A or A^*, and their standard deviations, SD_n, etc., can be estimated (Ref. 11) from

$$n = \frac{1}{\alpha} - 1 \tag{6}$$

$$SD_n \approx \frac{SD_\alpha}{\alpha^2} \tag{7}$$

$$D = 10^\beta$$

$$SD_D \approx 2.3026\left(SD_\beta\right)\left(10^\beta\right) \tag{8}$$

$$B = \frac{\alpha 10^{\beta/\alpha}}{\sigma_i^{1/\alpha-3}} \tag{9}$$

$$A^* = \frac{2K_{Ic}^2\left(\sigma_i\right)^{\frac{1}{\alpha}-3}}{10^{\beta/\alpha}(1-3\alpha)Y^2} = \frac{2K_{Ic}^2}{B(n-2)Y^2} \tag{10}$$

$$A = \frac{2K_{Ic}^{3-\frac{1}{\alpha}}\left(\sigma_i\right)^{\frac{1}{\alpha}-3}}{10^{\beta/\alpha}(1-3\alpha)Y^2} = \frac{2K_{Ic}^{2-n}}{B(n-2)Y^2} \tag{11}$$

where Y is the geometry correction factor for the stress intensity formulation. The crack depth to half-length ratio, a/c, was taken as 0.1 and the corresponding value of the geometry correction factor as $Y = 1.95$ where $K_I = \sigma Y\sqrt{a}$.

3.2 Window Stresses

During orbit, the windows are required to sustain an annual differential pressure spectrum of 0.93 MPa (135 psid) applied for 0.5 hours, followed by 0.21 MPa (30 psid) for 14.5 hours. The desired life of the windows is 10 years with an additional safety factor of 4×, leading to a 40 cycle loading spectrum and 600 hours under variable pressure.

The window is contained and supported on the periphery with a flexible seal, resulting in neither a completely fixed nor completely free boundary condition. If the boundary condition is taken as simply supported at the edge of the window and the window face presumed to be the *c*-plane, which is elastically isotropic, the stresses can be described by (Ref. 12):

$$\sigma_{rr} = \frac{3PR_s^2}{8t^2}\left[(1-\nu)\frac{R_s^2}{R_d^2} + 2(1+\nu) - (3+\nu)\frac{r^2}{R_s^2}\right] + \sigma_s \tag{12}$$

$$\sigma_{\theta\theta} = \frac{3PR_s^2}{8t^2}\left[(1-\nu)\frac{R_s^2}{R_d^2} + 2(1+\nu) - (1+3\nu)\frac{r^2}{R_s^2}\right] + \sigma_s \tag{13}$$

$$\sigma_s = \frac{P(3+\nu)}{4(1-\nu)} \tag{14}$$

where P is the applied pressure, R_S is the support radius, R_d is the window radius, t is the window thickness, ν is Poisson's ratio and r is the radius of interest. The term σ_s is a small correction factor to the simple plate theory for the effects of the shearing stresses and lateral pressure on the plate deflection (Ref. 13). Based on Equations (12) to (14), a pressure of 0.93 MPa (135 psid) and nominal dimension of 8 mm thickness, 115 mm support diameter, and 121 mm window diameter, the maximum stress is 60 MPa.

For orientations other than the *c*-plane, Equations (12) to (14) do not accurately describe the elastic stress distribution. The stresses based on a general displacement solution for an anisotropic plate subjected to pressure (Refs. 14 to 16) are shown in Figure 3(a) for a window with an *a*- or *m*-plane face. The anisotropy causes a variation in the radial and tangential stresses with circumferential position, particularly at the edge of the window. For comparison, the stresses in a window with a *c*-plane face are shown in Figure 3(b). The radial and tangential stresses do not vary with circumferential position.

4. Results

4.1 Fracture Toughness

Chevron-Notch Testing

Initial attempts to measure *a*- and *r*- fracture toughness by using the VB were complicated by poor test specimen machining. The poor machining resulted in the notch parameters α_1 and/or α_0 being slightly out of specification (see Fig. 4), and relatively wide notches (0.3 to 0.5 mm vs. 0.27 to 0.35 typically) for the *r*-plane specimens. ASTM C1421 (Ref. 4) does not require a minimum notch width; however, it recommends a width less than 0.300 mm in order to promote stability. To remedy the notch parameter deviations in estimation of the fracture toughness, specific stress intensity factor coefficients for the actual parameters were calculated, rather than using those calculated from the narrow range equations supplied in C 1421. These corrections were less than 1 percent and not significant for engineering purposes. The results for tests in air are summarized in Table 1. Some tests results are not included in Table 1 because they were either invalid or could not be accurately remedied. This was usually due to crack growth instability or specimen damage by the machinist. The instability was attributed the wide notches.

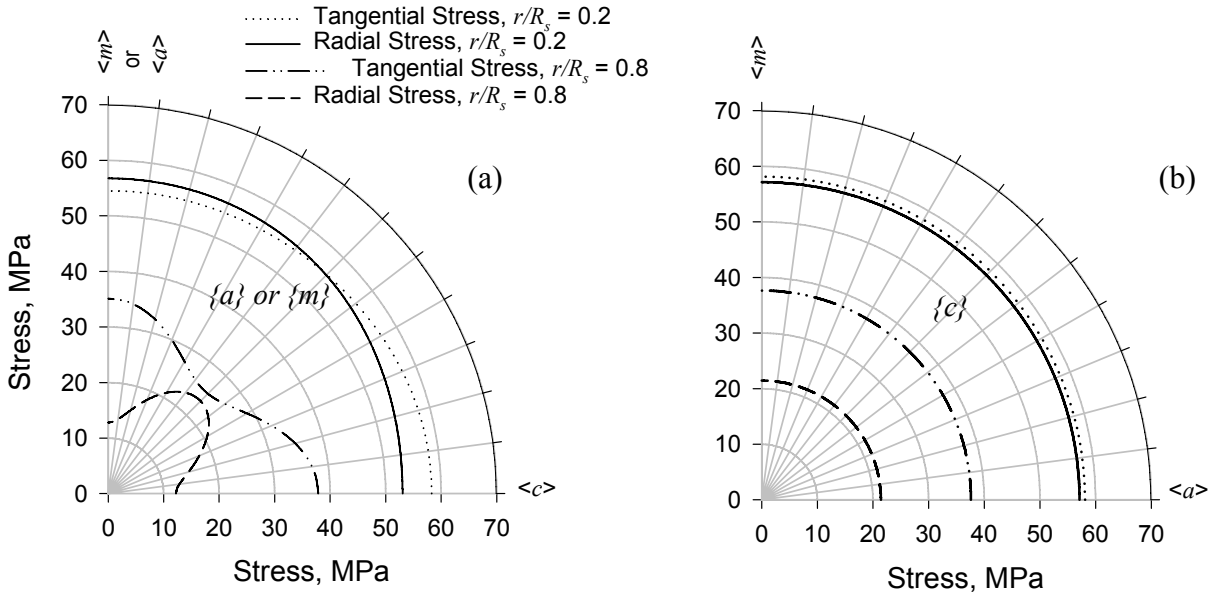

Figure 3.—Polar plot of the stresses in a 115 mm diameter, 8 mm thick, simply supported sapphire window subjected to a 0.93 MPa pressure: (a) window face is the *a*- or *m*-plane, and (b) window face is the *c*-plane.

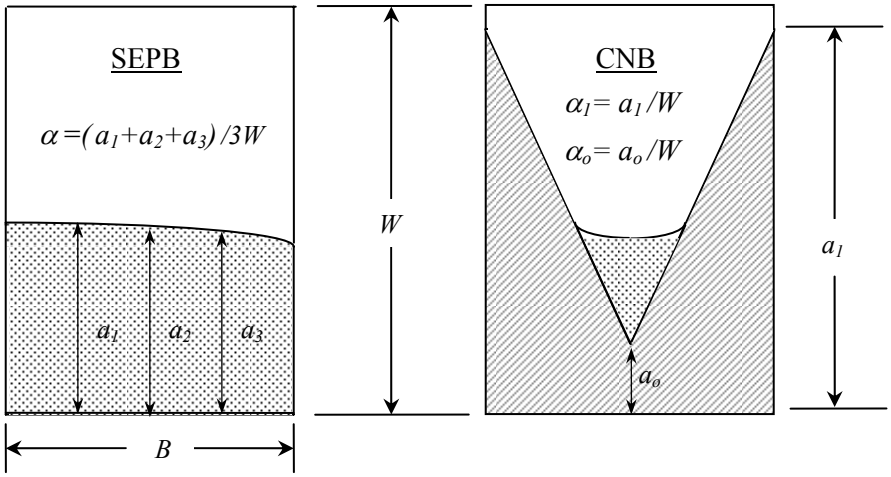

Figure 4.—Crack configurations and configuration for single-edge-precracked-beam and chevron-notch test specimens.

TABLE 1.—VB TEST RESULTS FOR 50 PERCENT RH AIR. RESULTS ARE FROM THE FIRST SET OF SPECIMENS MACHINED

Specimen Number	Test Condition	Measured Toughness, MPa√m	Noncompliant Values	Other Complications	Remedy
R58	50 percent RH	1.98	α_0 and α_1	Wide notch	Calculate *Y*
R60	50 percent RH	1.94	α_0 and α_1	Wide notch	Calculate *Y*
A57	50 percent RH	1.96	α_1	None	Calculate *Y*
A58	50 percent RH	1.96	α_1	None	Calculate *Y*
A59	50 percent RH	1.88	α_1	None	Calculate *Y*
A60	50 percent RH	1.84	α_1	None	Calculate *Y*
SiC JAS-A12	50 percent RH	2.60	None	α SiC Witness test	

In order to obtain more data than shown in Table 1, two tracks were taken: (1) additional test specimens were machined; and (2) the remnants of the VB test specimens were tested using the PB method. The second set of VB specimens conformed to the geometric requirement and the notches were narrower, however, the notch planes that form the chevron were occasionally offset slightly more than allowed in C1421. Despite the narrower notches, it was still difficult to attain stable extension as required, presumably due to the offset. In order to promote stable initiation, the specimens were loaded in compression several times and then tested in the usual manner, to no avail. A second unsuccessful attempt to get stability was performed by loading the specimens to near the expected initiation load and holding for several minutes to several hours. Finally, a PB precracking fixture was used to generate short precracks like those shown in Figure 5. This consistently resulted in stable extension as required, however, some of the precracks were longer than the crack length corresponding to minimum stress intensity factor coefficient, Y^*_{min}. This was remedied by calculating a specific Y^* value and pairing it with the corresponding load at the onset of stable extension. This generally lead to a lower measured fracture toughness than using the maximum load and minimum stress intensity factor coefficient (as is usually done), because the decrease in load was usually larger than the increase in Y^*, and because the crack velocity is lower than that occurring in a test with large, stable extension followed by unstable extension. The useful results are summarized in Table 2.

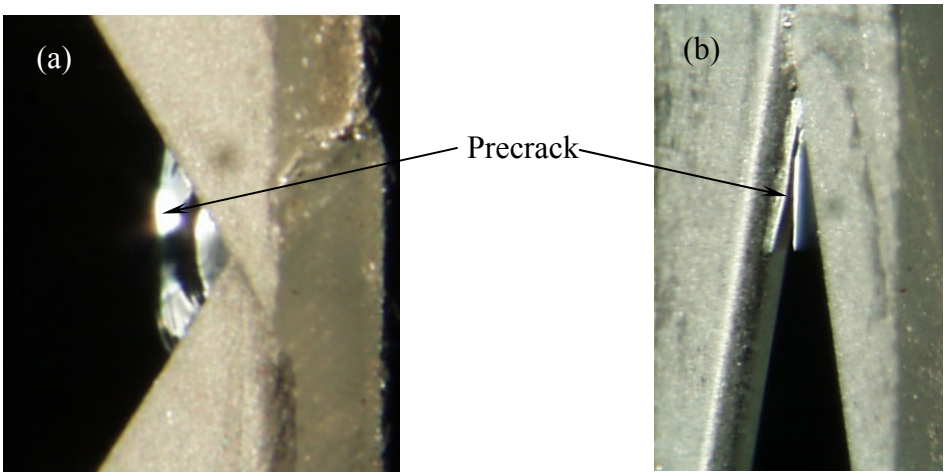

Figure 5.—Precracked VB test specimens showing the precrack as viewed through (a) the bottom, and (b) the side.

TABLE 2.—VB TEST RESULTS FROM THE SECOND SET OF SPECIMENS MACHINED. TESTS WERE CONDUCTED IN DISTILLED, DEIONIZED WATER AFTER SOAKING FOR 10 MINUTES

Specimen Number	Test Condition	Measured Toughness, MPa√m	Noncompliant Values	Other Complications	Remedy
A-II-4	Water	2.07	Notch plane offset	Long precrack	Calculate Y^*
M-II-4	Water	1.98		Semi-stable	
R-II-1	Water	1.82	Notch plane offset	Long precrack	Calculate Y^*
R-II-2	Water	1.80		Long precrack	Calculate Y^*
R-II-3	Water	1.87		Manual precracking	
R-II-4	Water	1.70		Long precrack	Calculate Y^*
R-II-5	Water	1.93	Notch plane offset	Manual precracking	
SiC JAS-A16	Air	2.58	None	α SiC Witness test	

As more test results than in Table 2 were needed, a third set of VB specimens was machined. These specimens meet all geometric tolerances, and the notch widths and offsets were excellent. Despite this, stable extension was difficult to attain.

This was speculated to be from residual stresses at the notch root, or a different grinding rate or wheel that left fewer micro cracks at the notch root. Communications with the machine shop indicated that the same wheel was used; however, the feed rate may have been slowed to improve the notch tolerances. To test the theory that residual stresses were hampering stable crack initiation, two *r*-plane specimens were annealed and tested along with the as-received specimens. Again stable extension could not be attained. Thus precracking was employed. This was successful, except for the annealed test specimens. These could not be precracked at the usual load, implying that healing of machining damage in the notch root hampers initiation of crack extension in the VB. The useful results for the third set are summarized in Tables 3 to 5.

During testing and data analysis, it was noted that well aligned, smooth precracks resulted in lower fracture toughness values, particularly for the *r*-plane, as shown in Figures 6 to 8 and noted in the comments in Tables A4 to A6 in the Appendix. Further fractography indicated that for the *r*-plane, cracks initiate on both sides of the chevron and join, resulting in a cleavage step. Depending on the steps, different values resulted (from 1.51 MPa√m for no steps to ~2.0 MPa √m for large or multiple steps), as shown in Figure 8. Specimens that fractured unstably from the chevron tip or during machining/handling exhibited a very planar surface with no cleavage steps visible to the unaided eye. The increase in measured fracture toughness for crack growth on planes even slightly misaligned with the *r*-plane is supported by recent dry nitrogen data (Ref. 17) and from early data in liquid nitrogen. The recent results indicated difficulty in keeping a crack on the *r*-plane and stress intensities greater than 2.8 MPa√m in dry nitrogen. The early results in liquid nitrogen indicated fracture energies of 6.2 to 8.7 J/m^2 (2.14 to 2.53 MPa√m) for a rough surface (Ref. 18), and were thought to be too large to represent extension on the *r*-plane.

All of the *a*-plane test specimens exhibited a smooth, conchoidal fracture surface without cleavage steps, as shown in Figure 6, implying that the fracture resistance on and near the *a*-plane is similar. Tilted precracks resulted in slight increase in the measured fracture toughness. The *m*-plane specimens occasionally exhibited poorly defined step-like features. When the precrack was tilted significantly, the measured fracture toughness was elevated 10 to 15 percent, as shown in Tables A4 to A6 in the Appendices.

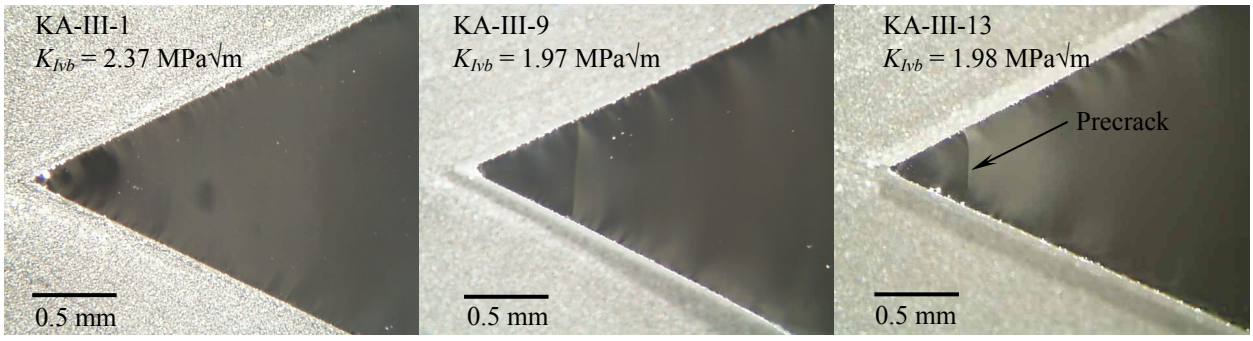

Figure 6.—Fracture surfaces of *a*-plane VB specimens tested in air or water.

TABLE 3.—VB *a*-PLANE TEST RESULTS FROM THE THIRD SET OF SPECIMENS MACHINED. THE SPECIMENS WERE TESTED IN AIR OR DISTILLED, DEIONIZED WATER AFTER SOAKING FOR 20 MINUTES

Specimen Number	Test Condition	Measured Toughness, MPa√m	Noncompliant Values	Other Complications	Remedy
KA-III-1	50 percent RH	2.37	None		
KA-III-2	50 percent RH	2.09	None	Long precrack	Calculate Y^*
KA-III-3	50 percent RH	2.33	None		
KA-III-7	Water	1.90		Long precrack	Calculate Y^*
KA-III-8	Water	1.95	None	Manual precracking	
KA-III-9	Water	1.97	None	Manual precracking	
KA-III-12	Water	1.96	None	Manual precracking	
KA-III-13	Water	1.98	None	Manual precracking	
KA-III-14	Water	1.96	None	Manual precracking	
SiC-JAS-A17	Water	2.63	None	α SiC Witness test	

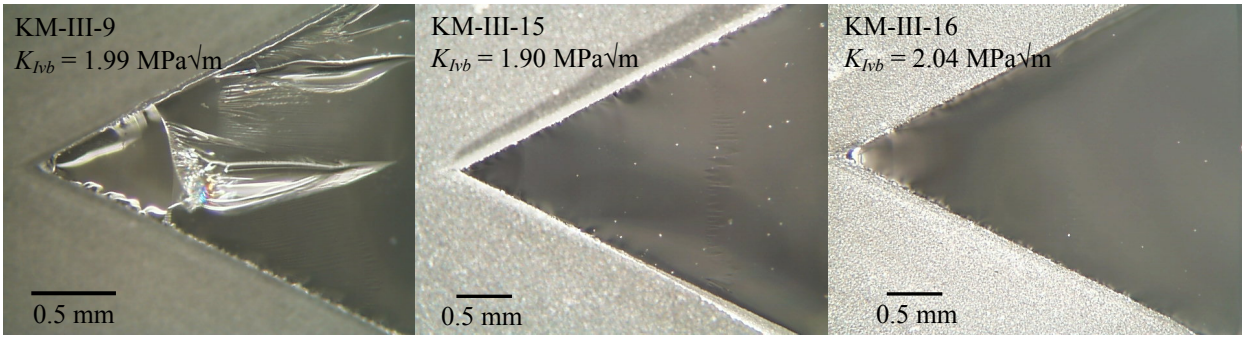

Figure 7.—Fracture surfaces of *m*-plane VB specimens tested in water.

TABLE 4.—VB *m*-PLANE TEST RESULTS FROM THE THIRD SET OF SPECIMENS MACHINED. THE SPECIMENS WERE TESTED IN DISTILLED, DEIONIZED WATER AFTER SOAKING FOR 20 MINUTES

Specimen Number	Test Condition	Measured Toughness, MPa√m	Noncompliant Values	Other Complications	Remedy
KM-III-7	Water	1.82	None	Long precrack	Calculate Y^*
KM-III-9	Water	1.91	None	Long precrack	Calculate Y^*
KM-III-10	Water	1.97	None	Manual precracking	
KM-III-12	Water	1.92	None	Long precrack	Calculate Y^*
KM-III-13	Water	1.95	None	Manual precracking	
KM-III-15	Water	1.90	None	Manual precracking	
KM-III-16	Water	2.04	None	Manual precracking	
KM-III-17	Water	2.01	None	Manual precracking	

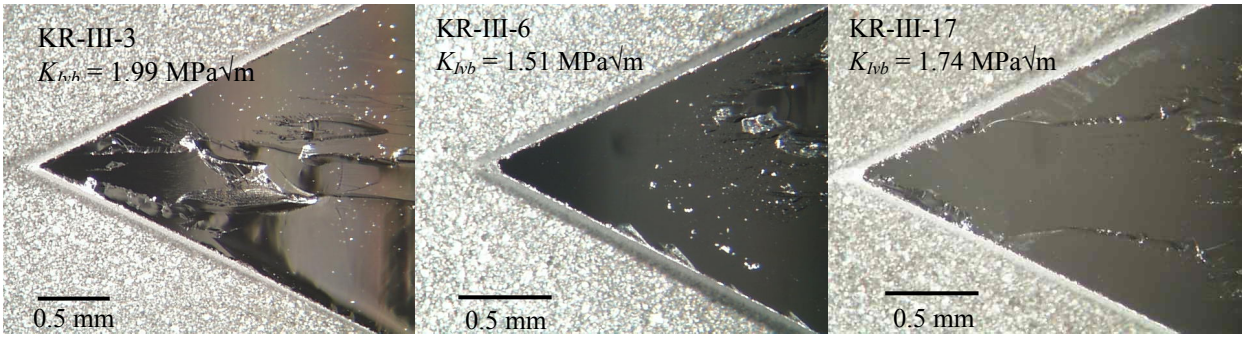

Figure 8.—Fracture surfaces of *r*-plane VB specimens tested in water.

TABLE 5.—VB *r*-PLANE TEST RESULTS FROM THE THIRD SET OF SPECIMENS MACHINED. THE SPECIMENS WERE TESTED IN DISTILLED, DEIONIZED WATER AFTER SOAKING FOR 20 MINUTES

Specimen Number	Test Condition	Measured Toughness, MPa√m	Noncompliant Values	Other Complications	Remedy
KR-III-3	Water	1.99	None	Manual Precracking	
KR-III-6	Water	1.51	None	None	
KR-III-12	Water	1.73	None	Long precrack	Calculate Y^*
KR-III-13	Water	1.70		Long precrack	Calculate Y^*
KR-III-16	Water	1.71	None	Manual Precracking	
KR-III-17	Water	1.74	None	Manual Precracking	
KR-III-18	Water	1.85	None	Manual Precracking	

Single-Edge-Precracked-Beam Testing

Precracking of the test specimens was performed in ambient laboratory air. Testing of the specimens was performed in high purity dry nitrogen or silicone oil after subjecting the precracked specimens to vacuum drying for ~20 hours. This was done to obtain a fracture toughness value in the absence of SCG, and thereby estimate a maximum value. Such an "inert" fracture toughness is needed to combine with the materials inert strength for estimation of the initial flaw size in the calculation of the SCG parameter *A,* and for estimation of the window proof test pressure. The crack extension and stability of the tests were monitored by a strain gage placed on the back-face of the test specimens (Ref. 19). The measured fracture toughness, K_{Ipb}, of the *r*-plane was 2.47±0.15 MPa√m for six valid tests. The measured fracture toughness, K_{Ipb}, of the *a*-plane was 2.31±0.12 MPa√m for ten valid tests. In total, 13 valid and invalid *r*-plane tests were run for a mean of 2.47±0.20 MPa√m, and 14 valid and invalid *a*-plane tests were tested for a mean of 2.32±0.16 MPa√m.

The precrack and fast fracture regions in the *r*-plane test specimens tended to be very planar, except when the precrack hooked or turned slight out of plane at the precrack front, as shown in Figures 9 and 10. This was likely due to frictional effects in the precracking fixture rather than to any tendency of the crack to transition to other planes because the same effect is observed in polycrystalline test specimens (Ref. 19). Very small cleavage steps emanated from the indentations used to initiate the precracks. The crack hook and steps were quite beneficial in that the crack length would otherwise be difficult to measure because penetrant did not wet the cracks well. The precracks in the *a*-plane test specimens tended to exhibit a conchodial appearance. Observations of fractured specimens with low magnification polarized light indicated an absence of twinning. In order to check for small scale twinning activity and dislocations, surfaces of two *a*- and two *r*-plane test specimens were etched by using sodium tetraborate, which is quite specific to *a*-planes, at 800 °C for ~20 to 60s. Only a few etch pits could be observed on the *a*-plane sides of the *r*-plane specimen, implying a very low dislocation density (~1000/cm^2) for this material. Observations on both sides of the precrack front on the fracture surface of the *a*-plane specimens indicated no increase in the dislocation density and thus little plastic deformation (Ref. 20). Also, no evidence of twins could be observed on the *r*-plane fracture surfaces, except at the indentations used to initiate the precracks. Thus the slight increase in measured fracture toughness of the *r*-plane specimens as compared to the *a*-plane may be due to the small cleavage steps or a small difference in cleavage energy in the absence of water.

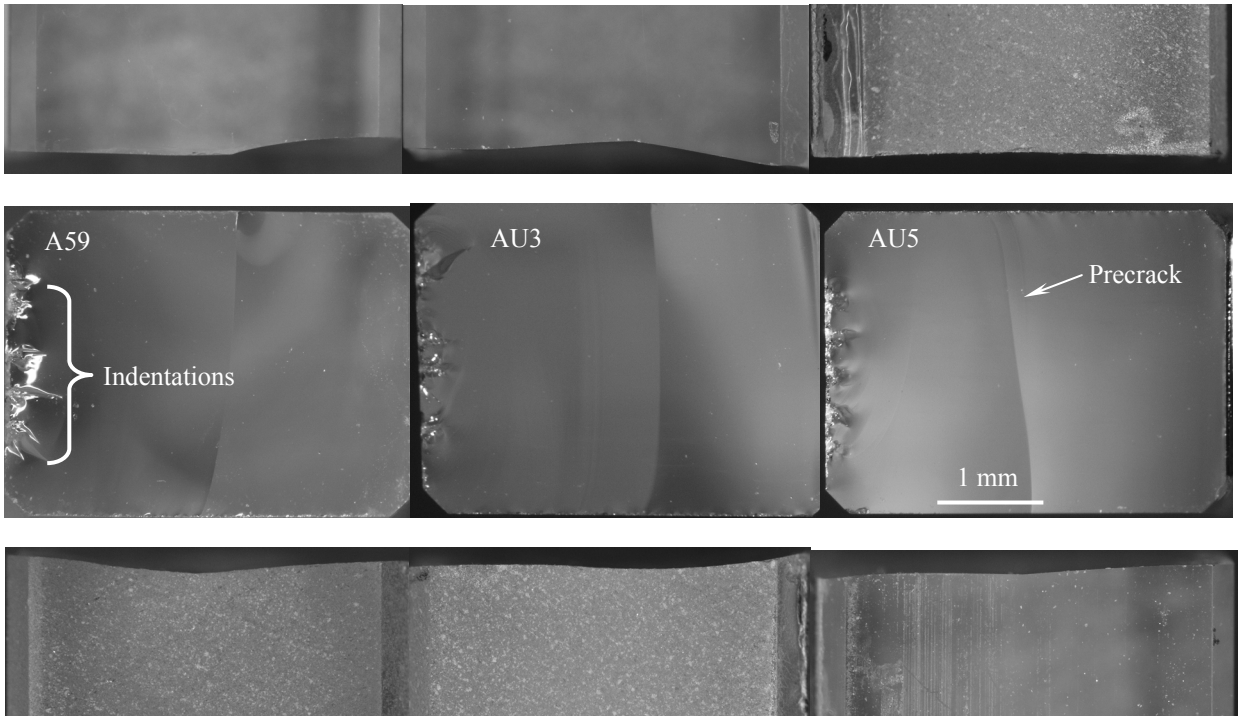

Figure 9.—Top and side views of the fracture surfaces of *a*-plane PB test specimens.

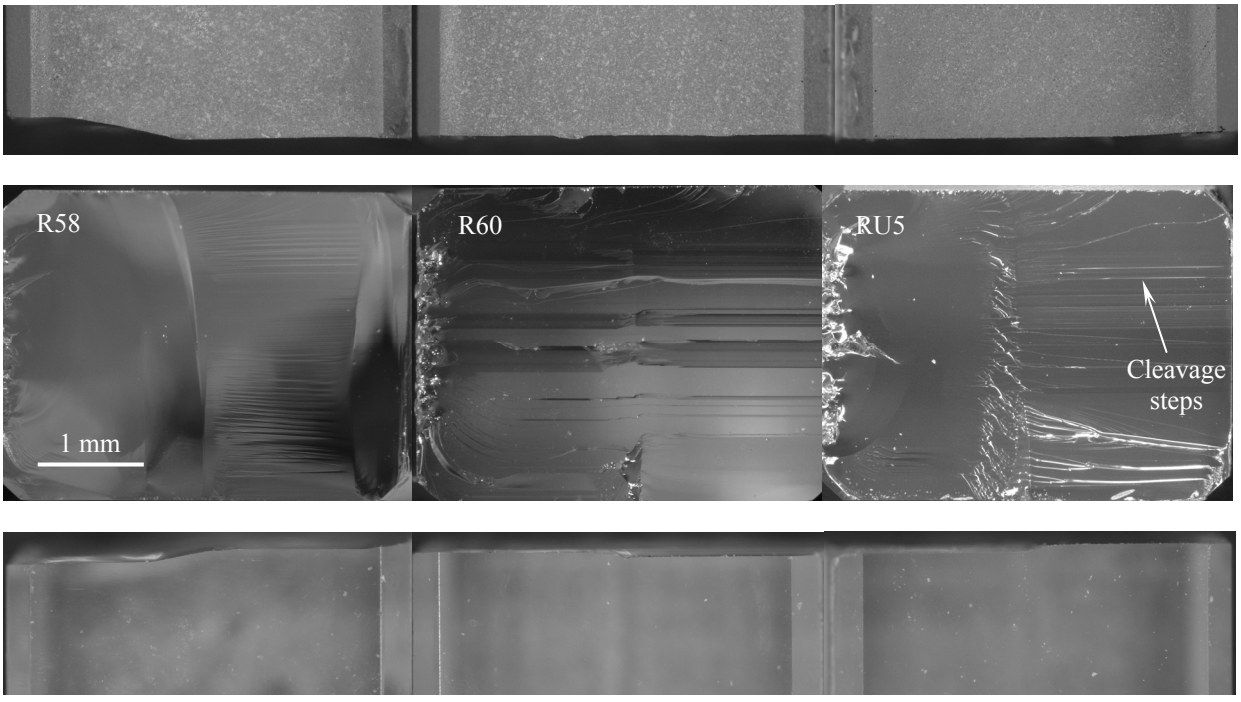

Figure 10.—Top and side views of the fracture surfaces of *r*-plane PB test specimens.

Comparison to Published Values

As mentioned previously, Wiederhorn and Krause (Ref. 17) reported difficulty in obtaining extension on the *r*-plane when using DT (double torsion) test specimens. However, double torsion measurements were successful on the *m*-plane and indicated values of 1.95 to 2.1 MPa√m in dry nitrogen at a velocity of ~10^{-4} m/s (Ref. 17). Although in this investigation, no such difficulty was encountered in producing very planar cracks in PB specimens, the PB and DT test method are quite different and in this study precracking was done in air. Evidently the susceptibility of the *r*-plane to cracking is very dependant on humidity. Other factors influencing fracture measurements may be impurities and residual stresses in the particular sapphire tested.

It should be noted that a fracture toughness value measured under stress corrosion conditions represents a point on the stress corrosion induced, crack growth curve and thus depends on the stress intensity rate and the ability of the corrosive medium to get to the crack tip, which depends on the concentration and crack size, etc. Thus the measured fracture toughness is an operational value based on a stated procedure. It is likely that the only stress intensities corresponding to fracture properties are the threshold value and that measured under inert conditions.

Table 6 summarizes data from published literature and this work. Most of the work indicates that the fracture toughness in dry nitrogen is greater than 2 MPa√m for all of the typical cleavage planes. The introduction of water to the environment drops the fracture toughness to just under 2 MPa√m for the *a*- and *m*-planes, however, for the *r*-plane the measured fracture toughness varies between 1.40 and 1.77 MPa√m depending on the test method and procedures (i.e. crack velocity) employed.

The large difference between the values on the *r*-plane may be due to the low *n* value and contaminant strong dependence on crack velocity, in addition to the flatness of the crack employed. As compared to polycrystalline alumina, sapphire exhibits substantially lower fracture toughness: For oil, air, and water a 96 percent polycrystalline alumina exhibited fracture toughness of 3.37±0.05, 3.19±0.07, and 2.75±0.01 MPa√m (Ref. 5), respectively.

For the *m*-plane, the measured fracture toughness in water is significantly larger than the threshold value in 85 percent RH air (1.94 vs. 1.65 MPa√m (Ref. 21)). The value reported by Reference 22 (2.33 MPa√m) was measured by using a relatively blunt saw notch (tip radius = 0.1 mm) and thus likely overestimates the fracture toughness of the *m*-plane in air, despite being lower than the value (3.14 MPa√m) measured by Iwasa and Bradt (Ref. 23) in air by using surface cracks. Many cleavage steps were observed on the fracture plane, implying propagation on multiple planes rather than on the *m*-plane only. For the *r*-plane, Michalske (Ref. 24) measured the crack velocity on the *r*-plane in water, ammonia, hydrazine, and acetonitrile. If the data is extrapolated to 10^{-4} m/s, a stress intensity of ~1.40 MPa√m is estimated for water, while a stress intensity >2.0 MPa√m is estimated for acetonitrile.

One troubling aspect of the reported data is the low values in Figure 23 of Reference 25. A fracture toughness of 1.62 MPa√m for the *r*-plane in dry nitrogen at 10^{-4} m/s is indicated in Figure 23; however, Table 4 of the same publication indicates much higher corresponding fracture energy of 0.6 J/m^2, which coverts to 2.10 MPa√m assuming isotropy and 2.18 MPa√m accounting for anisotropy. This difference nominally equates to √2 in the conversion. Private communication (Ref. 26) indicated the difference to be due to scatter. The *m*-plane fracture energy was reported as 7.3 J/m^2 (Refs. 18 and 25), which converts to 2.59 MPa√m assuming isotropy and E = 430 GPa, in agreement with a later publication reporting a fracture toughness of 2.5 MPa√m (Ref. 27).

It is critical that relatively planar cracks be generated, particularly for the *r*-plane, or elevated values will be measured. Further, environment and crack velocity play a strong role in the measured result, implying the need for a specific operational procedure or the use of threshold values.

TABLE 6.—REPORTED FRACTURE TOUGHNESS AND FRACTURE ENERGY OF SAPPHIRE. VALUES WITH REFERENCE NUMBER WERE THOSE REPORTED; THE CORRESPONDING FRACTURE TOUGHNESS OR FRACTURE ENERGY VALUES WERE CALCULATED BY ASSUMING ISOTROPY AND THE ELASTIC MODULUS OF THE ASSOCIATED DIRECTION AND A POISSON'S RATIO OF 0.26

Crystal plane	Fracture toughness, MPa√m	Cleavage energy, J/m^2	Elastic modulus, GPa
Water[a]			
a $\{\bar{1}2\bar{1}0\}$	1.95±0.03		
m $\{1\bar{1}00\}$	1.94±0.07		
r $\{10\bar{1}2\}$	1.77±0.13		
$r - v = 10^{-4}$	[b]1.40 (Ref. 24)		
Air[a]			
a - 50 percent RH	2.06±0.21		
r - 50 percent RH	1.96		
m - 85 percent RH; K_{Ith}	[c]1.64 (Ref. 21)		
m - 85 percent; $v = 10^{-4}$	[d]2.22 (Ref. 21)		
c $\{0001\}$	4.54±0.32 (Ref. 23)	21.54	465
m	3.14±0.30 (Ref. 23)	11.43	430
a	2.43±0.26 (Ref. 23)		430
r	2.38±0.14 (Ref. 23)	7.68	[e]440
m	2.33±0.07 (Ref. 22)		
Dry Nitrogen[a]			
a	2.31±0.12		
r	2.47±0.15		
$m - v = 10^{-4}$	[f]2.14 (Ref. 17)		
c		>40 (Ref. 18)	
m	[g]2.59±0.29	7.3±1.1 (Refs. 18 and 25)	430
r	[g]2.10±0.17	6.0±0.6 (Refs. 18 and 25)	344
$r - v = 10^{-4}$	[i]1.62	(Ref. 25)	
r –196 °C ℓN_2		24.0 (Ref. 28)	
$\{\bar{1}\bar{1}26\}$		24.4 (Ref. 28)	
$\{\bar{1}\bar{1}26\}$–196 °C ℓN_2		32.2 (Ref. 28)	
$\{\bar{1}\bar{1}23\}$–196 °C ℓN_2		16.4 (Ref. 28)	

[a]Room temperature unless stated otherwise.
[b]Value taken from Figure 2 of Reference 24 corresponding to a velocity of 10^{-4} m/s in water.
[c]Threshold stress intensity in 85 percent RH.
[d]Value taken from Figure 4 of Reference 21 corresponding to a velocity of 10^{-4} m/s in water.
[e]A value of E = 440 GPa was reported by Iwasa (Ref. 23) for the *r*-plane. E is closer to 344 GPa and thereby gives 7.68 J/m^2.
[f]Calculated from Equation (5) of Reference 17.
[g]Calculated from the formula $K_{Ic} = \sqrt{(2\gamma E/(1 - \nu^2))}$. Nineteen tests were on conducted on two anneal boules. Testing of unannealed boules resulted in 5.3±1.3 J/m^2.
[h]If anisotropy is considered, the *r*-plane value becomes 2.18 MPa√m.
[i]Value taken from Figure 23 of Reference 25 corresponding to a velocity of 10^{-4} m/s in dry N_2.

4.2 Non-Destructive Inspection

The optical inspections of the strength test specimens indicated a relatively well-polished gage section on both the *a*- and *r*-plane test specimens. However, the bevels of the *a*-plane test specimens were generally marked more strongly with grinding/polishing scratches than the *r*-plane test specimens, as shown in Figure 11. X-ray topographs indicated not only stronger grinding marks on the *a*-plane specimens, but also a "short" finish (i.e., insufficient material removal for elimination of the damage generated in the early grinding stages), as shown in Figures 12 and 13. Besides the remnant grinding damage, both the *a*- and *r*-plane test specimens exhibited asymmetric polishing of the tensile face bevels as shown in Figure 13. In discussions, the vendor[2] indicated that preparation of the *a*-plane specimens is more difficult due the hardness anisotropy of sapphire. Further, the vendor indicated that the polishing procedures used were developed for plates and lenses instead of narrow beams. This is collaborated by X-ray topographs of three disk test specimens that are shown in Figure 14. The disks were polished by the vendor at a similar time to the same specifications (60/40 scratch/dig) as the beam test specimens; however, they exhibit a much better finish.

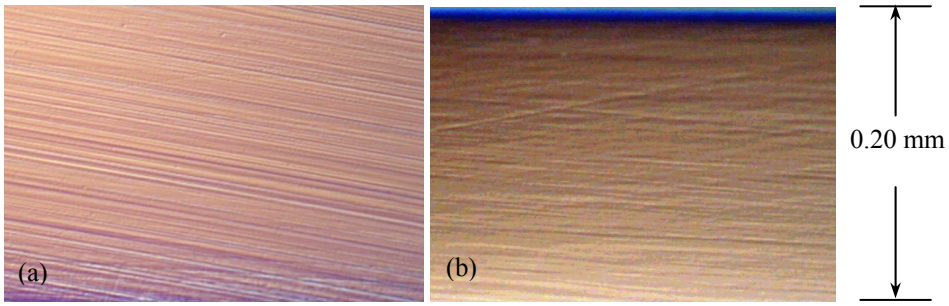

Figure 11.—Optical macrographs of (a) *a*-plane, and (b) *r*-plane test specimen bevels. The observations were made at 200×.

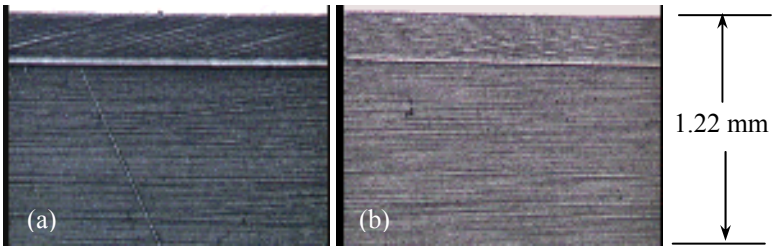

Figure 12.—X-ray topographs of (a) *a*-plane, and (b) *r*-plane test specimens.

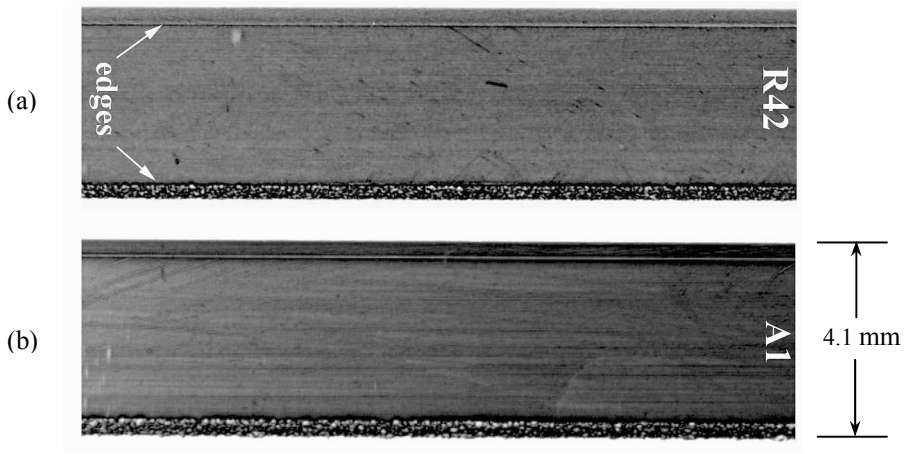

Figure 13.—X-ray topographs of the tensile face of (a) an *r*-plane test specimen and (b) an *a*-plane test specimen. Note the asymmetric bevel finish on both test specimens.

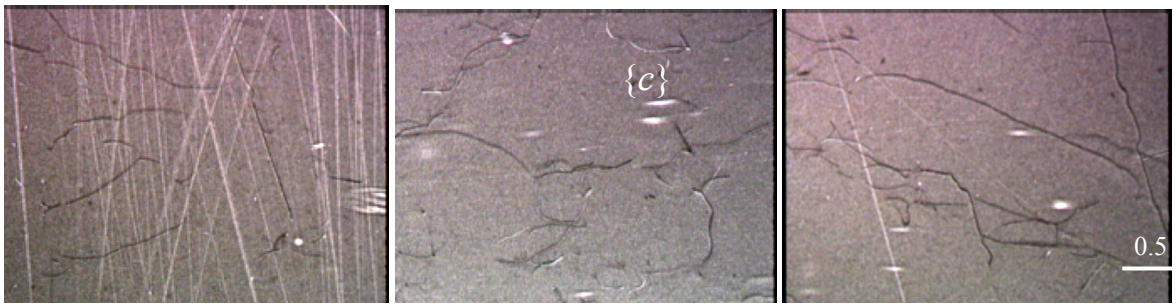

Figure 14.—X-ray topographs of the faces of three 50.4 mm disk test specimens showing a near dislocation level finish. The face of the disks is the *c*-plane.

4.3 Slow Crack Growth and Inert Strength Testing: *r-plane Data*

Weibull distributions of fracture strength in dry nitrogen and water at the slowest and fastest stress rates are plotted in Figure 15, and the fracture strength as a function of stress rate is plotted in Figure 16. A significant loss in strength is exhibited as the stress rate is reduced, implying stress corrosion induced crack growth. The SCG parameters corresponding to the data in Figures 15 and 16 are summarized in Tables 7 and 8, and the data is given in detail in Table A8 of the appendix. The *r*-plane of HEM sapphire exhibits a relatively low value of the fatigue exponent *n*, which is comparable to that of glass (Ref. 29).

The inert strength and SCG data exhibit four low out-lying data points that tend to skew the slope of the SCG curve because they occur so infrequently. One approach to minimize these points is the median deviation technique (Ref. 10), in which regression is performed by using the median fracture strength at each stressing rate. Unfortunately, ASTM C 1368 does not currently provide for the application of this technique. It is likely that the outlying values are associated with the bevels of the flexure specimens: a geometric feature that is less likely to influence the failure of a window because the stresses at the beveled edge of a window are lower than the stresses at the window center. The effect of censoring the outlying data points is shown in Figures 17 and 18 to illustrate what better polishing, handling, and inspection might achieve. If the outlying values were associated with bevel damage, then the censored fatigue parameters would be a better estimate of the SCG behavior. However, fractographic justification is needed for censoring. Without supporting fractography, which is left to future work, the uncensored SCG parameters should be considered the best estimates.

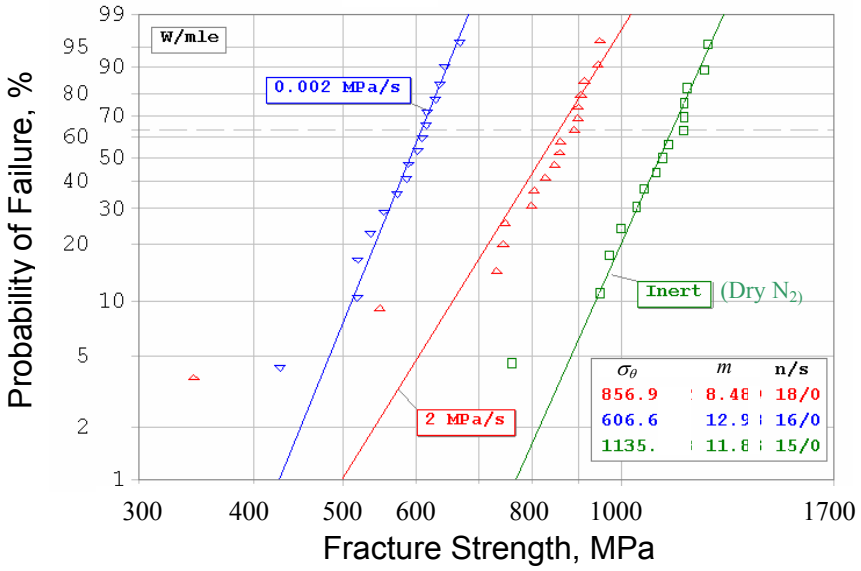

Figure 15.—Uncensored *r*-plane Weibull strength distributions for dry nitrogen and the slowest and fastest stress rates in water.

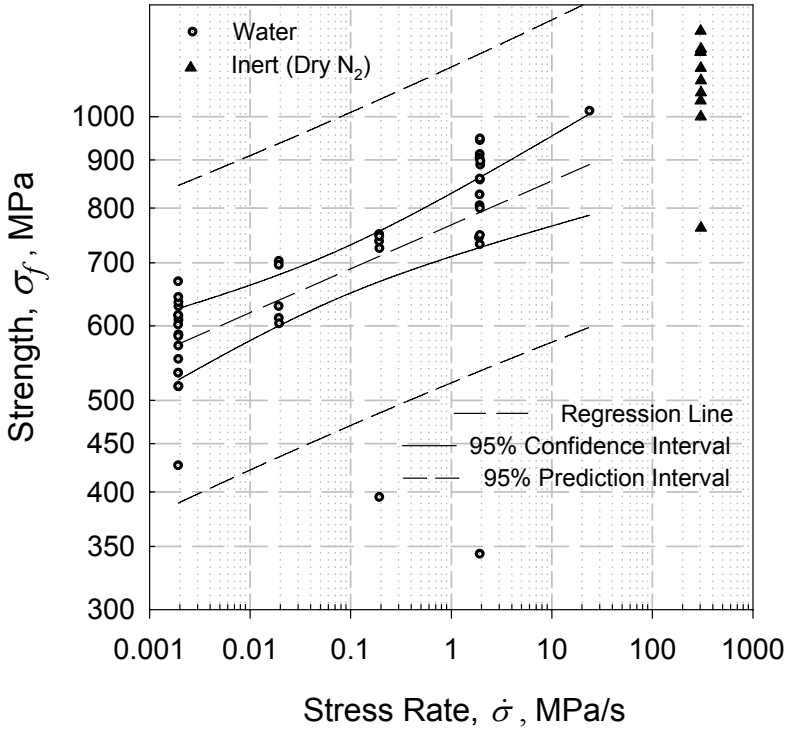

Figure 16.—Experimentally measured failure stress as a function of stress rate for the *r*-plane of sapphire in water.

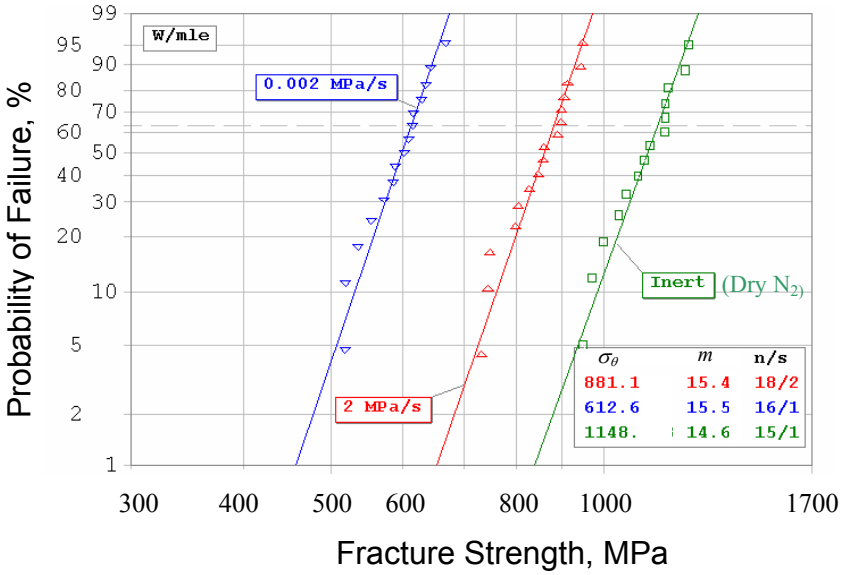

Figure 17.—Weibull strength distributions for the *r*-plane in dry nitrogen and for the slowest and fastest stress rates in water. Four outlying data points were censored.

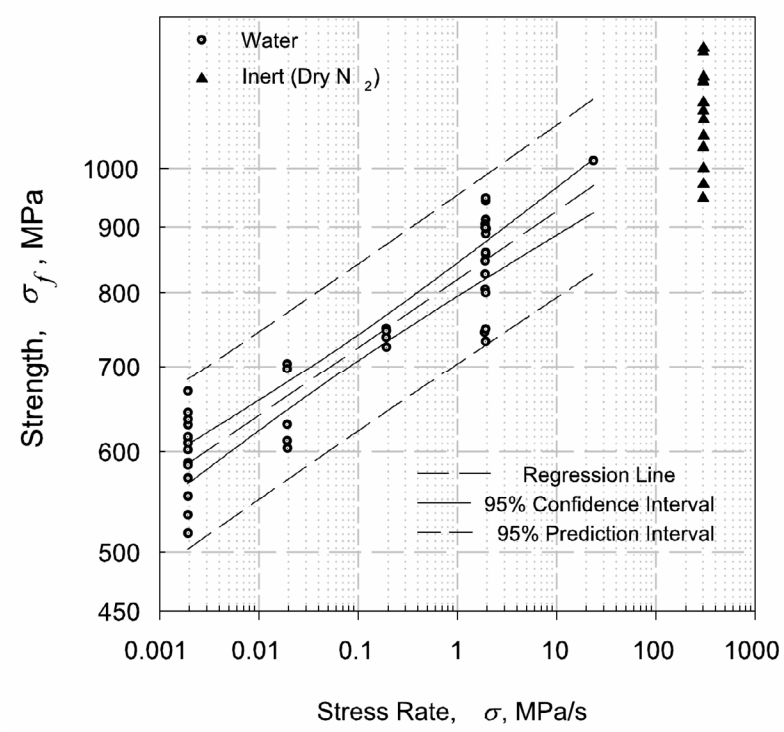

Figure 18.—Experimentally measured failure stress as a function of stress rate for the *r*-plane of sapphire in water. Four outlying specimens were censored.

TABLE 7.—MEASURED STRENGTH STATISTICS AND 90 PERCENT CONFIDENCE BANDS FOR THE *r*-PLANE

Stress Rate MPa/s (Number)	Mean Strength.[a] MPa	Characteristic Strength, σ_θ MPa	90 percent Confidence Bands on σ_θ	Weibull Modulus *m*	90 percent Confidence Bands on *m*
Uncensored Data:					
300 – Dry N_2 (15)	1085±127	1135	1093; 1179	12	8.5; 16
2 (18)	806±150	857	817; 899	8.5	6.3; 11
0.002 (16)	582±61	607	587; 627	13	9.4; 18
Censored Data:					
300 – Dry N_2 (14)	1108±93	1149	1113; 1186	15	10; 21
2 (16)	851±69	881	857; 906	15	11; 21
0.002 (15)	592±46	613	595; 630	16	11; 22

[a]± one standard deviation.

TABLE 8.—SLOW CRACK GROWTH PARAMETERS AND STANDARD DEVIATIONS FOR THE *r*-PLANE

Parameter	*n*	*D*	*B* MPa^2s	*A** m/s	*A* $m/s\cdot(MPa\sqrt{m})^{-n}$
Least Squares, All Data	21.0±4.4	762±28	24,454	7.12×10^{-6}	2.81×10^{-14}
Least Squares, Censored	17.7±1.3	819±12	251,204	8.38×10^{-7}	6.29×10^{-14}
Median Deviation	17.6±2.4	267±7	209,276	1.01×10^{-6}	9.43×10^{-14}

4.4 Slow Crack Growth and Inert Strength Testing: *a*-plane Data

The Weibull distributions and SCG data for the *a*-plane test specimens are shown in Figures 19 and 20. The data is extremely scattered, and the corresponding confidence in the SCG parameters is thus low. The source of scatter observed at any stress rate is likely the "short" finish and the asymmetric bevel polishing. Such scatter is common is sapphire, and although treatments such as "super polishing" and "annealing" significantly improved the mean strength of sapphire, such treatments did not decrease the scatter and increase Weibull modulus in one case reported in the literature (Ref. 30).

During testing, two test specimens (A23 and A32) failed while preloading and were thus subjected to very little slow crack growth. This was an unexpected occurrence because the *r*-plane, which was tested first, was reasonably consistent and strong, and the *a*-plane is generally considered tougher than the *r*-plane. The treatment of these data points has a strong influence on the SCG results but relatively little on the Weibull statistics for a specific stress rate. Three scenarios can be envisioned for processing of the data: (1) Censor the two test results because they are not representative of the slow crack growth process; (2) Use the data at the stress rate for which the tests were to proceed (i.e. treat them as upper bound

estimates of the SCG strength at the assigned stress rate); (3) Assign the data a stress rate based on the actual preloading rate. Scenario (1) seems the most plausible because the two tests are not representative of SCG due to the very short failure times. However, from a statistical sampling standpoint, case (2) seems appropriate because a slightly lower preload would have allowed measurement of a SCG strength. Case (3) seems implausible because the failure time is so short (< 2s) that the results likely approach inert strength measurements.

Tables 9 and 10 summarize the Weibull and SCG statistics associated with *a*-plane for all three scenarios. The detailed data is given in detail in Table A9 of the appendix. The parameter *n* varies from 31 for scenario (2) to 83 for scenario (3). Considering the relatively low values for SCG parameters for the *r*-plane ($n = 21$), it is suggested that *n* be taken as 31. Again, better test specimen preparation would eliminate the problems encountered in estimation of the SCG parameters for the *a*-plane.

TABLE 9.—MEASURED STRENGTH STATISTICS AND 90 PERCENT CONFIDENCE BANDS FOR THE *a*-PLANE.

Stress Rate MPa/s (Number)	Mean Strength[a] MPa	Characteristic Strength, σ_θ MPa	90 percent Confidence Bands on σ_θ	Weibull Modulus *m*	90 percent Confidence Bands on *m*
300 – Dry N_2 (15)	1255±547	1416	1195; 1677	2.64	1.89; 3.67
23 (19)	1078±456	1214	1047;1408	2.67	1.99; 3.58
0.002 (21)	785±334	888	769; 1024	2.63	1.99; 3.49

[a]± one standard deviation.

TABLE 10.—SLOW CRACK GROWTH PARAMETERS AND STANDARD DEVIATIONS FOR THE *a*-PLANE

Scenario	*n*	*D*	*B* MPa^2s	*A** m/s	*A* $m/s\cdot(MPa\sqrt{m})^{-n}$
(1)	37±23	887±66	93.5	8.26×10^{-4}	5.35×10^{-17}
(2)	31±16	868±66	499	1.89×10^{-4}	2.06×10^{-15}
(3)	83±112	832±63	2.45×10^{-8}	$1.37 \times 10^{+6}$	4.62×10^{-24}
Median Deviation	25±26	324±56	27,686	4.26×10^{-6}	5.55×10^{-15}

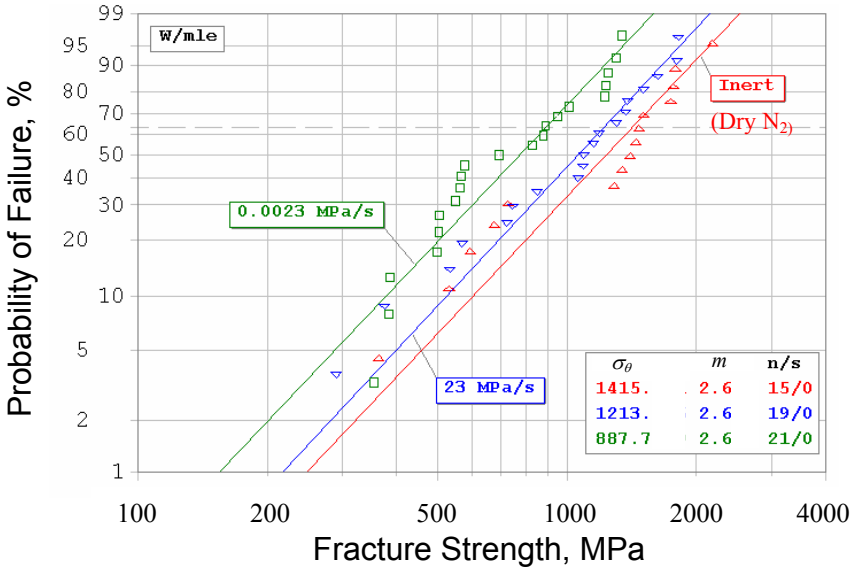

Figure 19.—Uncensored *a*-plane Weibull strength distributions for dry nitrogen and for the slowest and fastest stress rates in water.

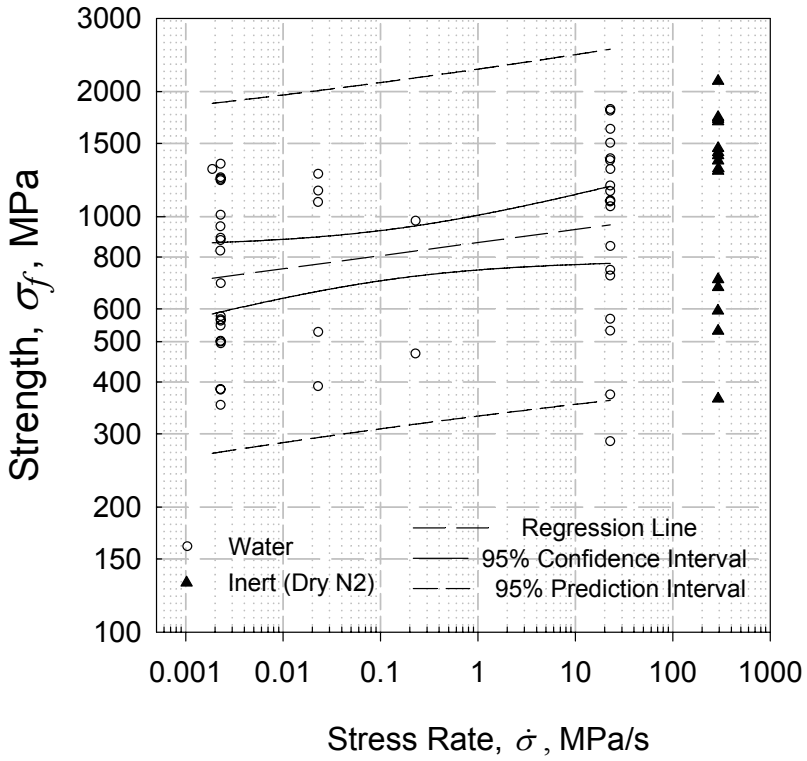

Figure 20.—Experimentally measured failure stress as a function of stress rate for the *a*-plane of sapphire in water.

Comparison to Published Literature

Table 11 and Figure 21 summarize data from this work and the literature. Some references did not report the SCG parameters and the original data was not available (Ref. 31), so the data was estimated by scanning and digitizing original reprints with commercial software[4]. In some cases, the digitized data was plotted on the same scale and size plot as the original figure, and overlaid on the original to assure that the process was accurate. The crack growth parameters A and n were determined by linear regression of log v as a function of log K_I.

The *a*-plane and *m*-plane data exhibit similar trends regardless of the humidity, with peak stress intensity of just over 2 MPa√m. The *r*-plane data varies widely. In general, older vintage data exhibits slow crack growth at lower stress intensities and much scatter as a function of RH (relative humidity). If a √2 adjustment is applied to the early NIST data, the agreement is better, but a significant difference still exists between recent NIST data (Ref. 17) and early NIST/Sandia data (Refs. 24 and 25). Dynamic fatigue testing resulted in lower n values than macro-crack techniques, and thus indicates more sensitivity to water vapor. The estimation of parameter A from the dynamic data requires an estimate of the initial flaw size distribution. This is estimated via the strength and fracture toughness measured in an inert environment (e.g., dry nitrogen or silicone oil). Figure 23 shows the sensitivity of the SCG curve on the inert fracture toughness. Even reducing the inert fracture toughness to 1.75 MPa√m does not make the *r*-plane data agree.

Based on the fractography of Reference 17, the *r*-plane of sapphire does not cleave easily in the absence of water vapor. Both large and small scale cracks (i.e., those from DT and dynamic fatigue test, respectively) exhibited extension at small angles (5 to 10°) to the *r*-plane on which the resolved mode I stress intensity is lower. In macro-crack DT test specimens, stable extension off the *r*-plane at very large stress intensities was followed by crack jumps onto the *r*-plane and a drop in the stress intensity to 2.8 MPa√m. In the dynamic fatigue specimens, a smooth mirror region followed by a rough surface was exhibited, implying stable extension and unstable extension off the *r*-plane prior to fast fracture. Two possible explanations for the crack not readily propagating on the *r*-plane are misalignment of the DT fixture and bend-twist coupling. Discussions indicated that misalignment was likely not the case (Ref. 32). Bend-twist coupling occurs in anisotropic materials, like sapphire, when insufficient symmetry occurs, as might be the case when the secondary orientation of the test specimen is not controlled. Other possibilities include residual stresses, which were noted to decrease fracture energy from 7.3±0.9 J/m^2 to 5.6±0.6 J/m^2 (23 percent) (Ref. 18), and cation dopant level, which increased the fracture toughness for 0.049 percent Ti^{3+} or Ti^{4+} on the *a*- and *m*-planes (Ref. 33). Results of Cr^{3+} doping were less clear.

[4]Un-Scan-It 5.0, Silk Scientific, P.O. Box 533, Orem, UT 84059

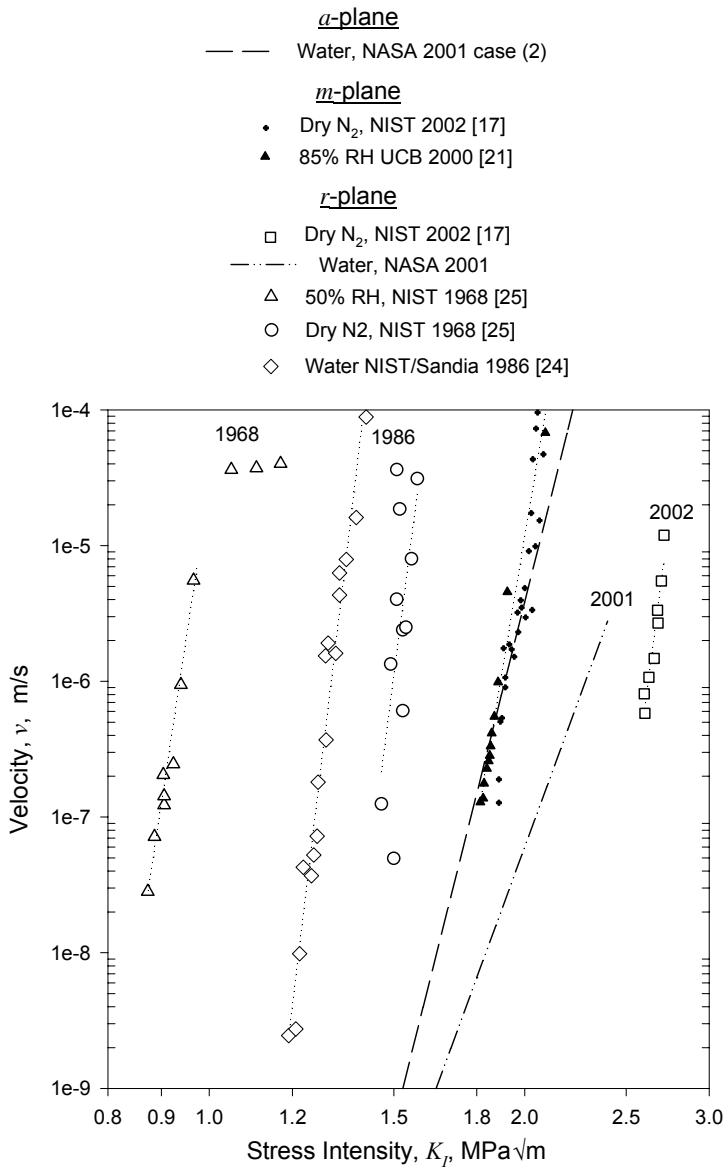

Figure 21.—Crack velocity as a function stress intensity factor for sapphire.

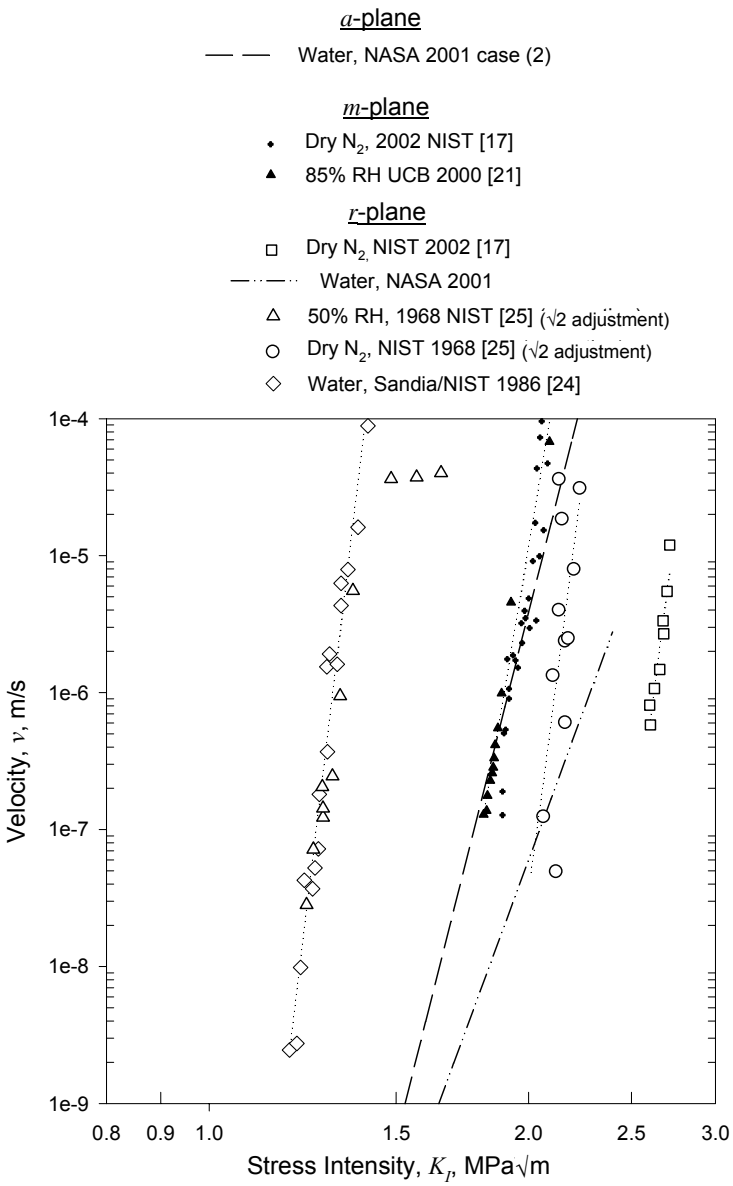

Figure 22.—Crack velocity as a function stress intensity factor for sapphire. A √2 factor was applied to the NIST 1968 data sets.

TABLE 11.—CRACK GROWTH PARAMETERS FOR SAPPHIRE IN AIR, WATER AND DRY NITROGEN

Data Source (number of data points)	Test Method[1]	A m/s (MPa$\sqrt{m}$)$^{-n}$	$n \pm SD_n$	Nominal Vintage & Growth Method[1]
		***a*-plane**		
This work	4 PB, Water	2.06×10^{-15}	31±16	2001, HEM[7]
		***m*-plane**		
(Ref. 21), As reported in text	CT, 85% RH	1.8×10^{-20}	45.6±2.5	2000, EFG[8]
(Ref. 17), Fig. 4, Data points[2]	DT, Dry N_2	1.44×10^{-21}	52.0±4.3	2002, EFG[9]
(Ref. 17), Eq. 5, 20 °C	DT, Dry N_2	1.11×10^{-21}	51.5	2002, EFG[9]
		***r*-plane**		
(Ref. 25, private) Fig. 23 (8)[3]	DCB, 50% RH	2.22×10^{-5}	49.7±4.1	1968, Verneuil[10]
(Ref. 25, private) Fig. 23 (11)[4]	DCB, Dry N_2	3.98×10^{-17}	59.6±26	1968, Verneuil[10]
(Ref. 24), Fig. 2, Data points (17)[5]	DCB, Water	3.18×10^{-14}	64.4±3.5	1986[11]
This work	4 PB, Water	2.81×10^{-14}	21.0±4.4	2001, HEM[7]
(Ref. 17), Fig. 7, Data points (8)[6]	DT, Dry N_2	3.88×10^{-32}	60.6±6.8	2002, EFG[9]

1. CT =compact tension; DT = double torsion; DCB = double cantilever beam; 4PB = four-point bend, HEM = heat exchange method; EFG = edge-defined film-fed growth.
2. The value of A was not reported, thus the data was digitized and fit. The reported average n for four measurements on three test specimens at 20 °C was 54.5±11.9.
3. The estimated standard deviation of log(A), $SD_{log(A)} = 0.17$. Propagation of errors gives $SD_A = 2.3026\ A\ (SD_{log(A)}) = 8.68 \times 10^{-6}$.
4. The estimated standard deviation of log(A), $SD_{log(A)} = 4.81$. Using propagation of errors gives $SD_A = 4.41 \times 10^{-16}$.
5. The estimated standard deviation of log(A), $SD_{log(A)} = 0.39$. Using propagation of errors gives $SD_A = 2.83 \times 10^{-14}$.
6. The estimated standard deviation of log(A), $SD_{log(A)} = 1.57$. Using propagation of errors gives $SD_A = 2.58 \times 10^{-31}$.
7. Manufactured by Crystal Systems, Salem, MA with the HEM (Heat-Exchange Method).
8. Manufactured by Kyocera, with the EFG (Edge-defined, Film-fed Growth) method.
9. Manufactured by Saphikon Inc./St. Gobain, Milford NH, with EFG.
10. Manufactured by Linde Corp by the Verneuil method.
11. Manufactured by Atomergic Chemetals Corp., Plainview NY, probably by EFG.

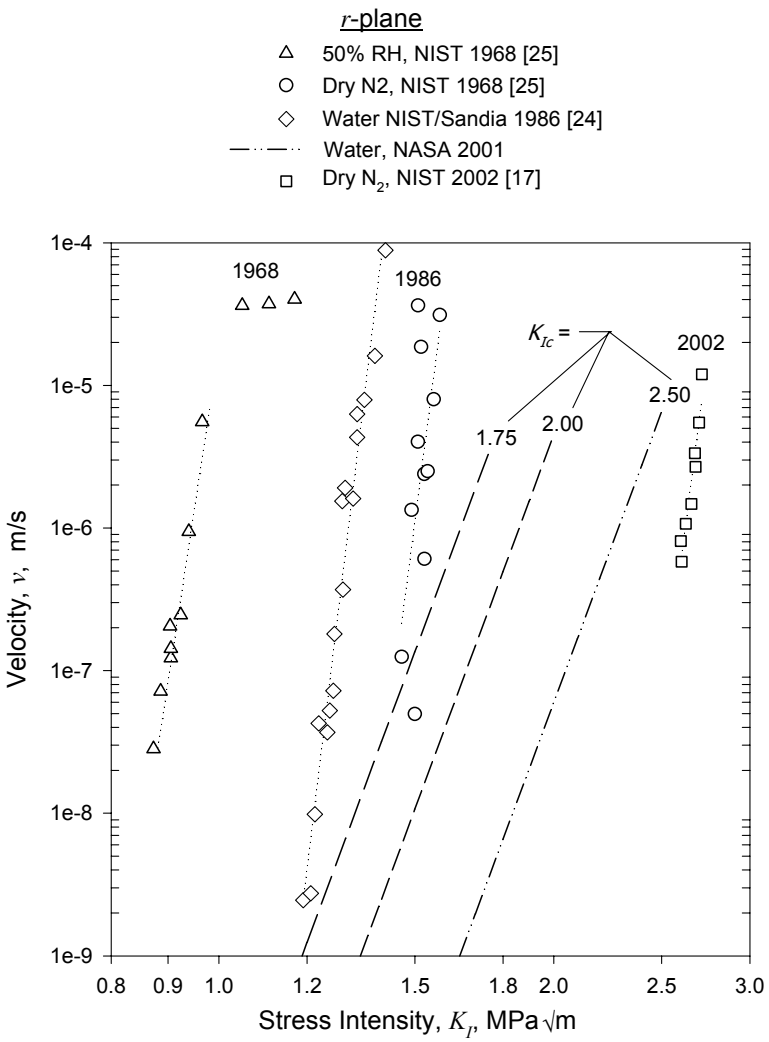

Figure 23.—Crack velocity as a function stress intensity factor for the *r*-plane of sapphire. The effect of the value of inert fracture toughness used to estimate the SCG curve is shown for constant stress rate data from *r*-plane test specimens.

4.5 Fractographic Observations

Casual observation of the test specimens during testing indicated failure from origins located on both the bevels and within the tensile face gage section. However, during the strength testing, occasional pops were heard and jumps in the load–time recordings were noted. In an initial set of inert strength tests (10 *r*-plane specimens and 10 *a*-plane specimens) none of the load drops were sufficient (10 percent load drop within 10 milliseconds) to trigger the test systems "break detect" function and unload the test specimen. However, in a second set of tests (5 *r*-plane specimens and 5 *a*-plane specimens) one inert, *r*-plane test that triggered the detector prior to failure displayed cracks running between the compressive face to the neutral axis, as shown in Figure 24. The cracks developed from twins that run between the compressive face and the neutral axis (Ref. 34). As the material to the left of the twins tried to move upward relative to that to the right, the cracks formed at the neutral axis and propagated upward as the faulted material is squeezed out. The faults were relatively uniformly distributed within and just outside the inner load span. No damage on the tensile surface was apparent to the unaided eye and the specimen remained whole. Apparently, failure under inert conditions occurs by two competing effects: (1) tensile

face fracture from large flaws prior to significant twining; and (2) tensile face fracture after severe twin faulting has diminished the ability of the compressive section to bear load, thereby shifting the test specimen neutral axis and elevating the tensile face stress. Thus, tensile face failure origins are observed despite the formation of twins. The audible pops and load-drops are probably the result of the faults forming and the material popping-out of the compressive side of the gage section. The result of twinning is likely a lower measured strength. The use of graphite foil, which has been reported to suppress compression face twins and increase strength (Ref. 8), was not sufficient in this case. Polishing of the compressive side of the test specimens should minimize the formation of the compression-side twins during inert strength testing.

Testing in water at lower stress rates (2 MPa/s for 15 *r*-plane specimen and at 23 MPa/s for 15 *a*-plane specimens) did not result in load drops sufficient to trigger the break detect for an initial set of test specimens. As the stress level at failure is lowered and the environment made more corrosive, SCG becomes the dominant failure mechanism. However, during testing of three *r*-plane specimens 7 months later and four *a*-plane specimens 1 month later, one *r*-plane test specimen (R61) and one *a*-plane test specimen (A49) triggered the break detect. Additional fractography of *r*-plane specimens indicated the presence of many twins in the compression region of all but two specimens (R3 and R18). The frequency and delineation of twinning was dependant on the stress level, with the number of twins ranging from ~one dozens at ~500 MPa to nearly one hundred at 1 GPa. The fracture mirror and trace along the tensile face appeared parallel to the *r*-plane; however, the surrounding planes containing river marks were consistently at a ~26° to the *r*-plane (Figure 25(a)). The line of intersection between the *r*-planes and the *a*-plane sides is normal to the *c*-plane twins, implying that the *r*-plane mirror transits onto the *m*-plane. This is consistent with the lower inert fracture toughness for the *m*-plane as compared to the *r*-plane. No distinct bifurcation occurred, however, at distances well away from the origin, bifurcation-like cracks were apparent (Fig. 25(b)).

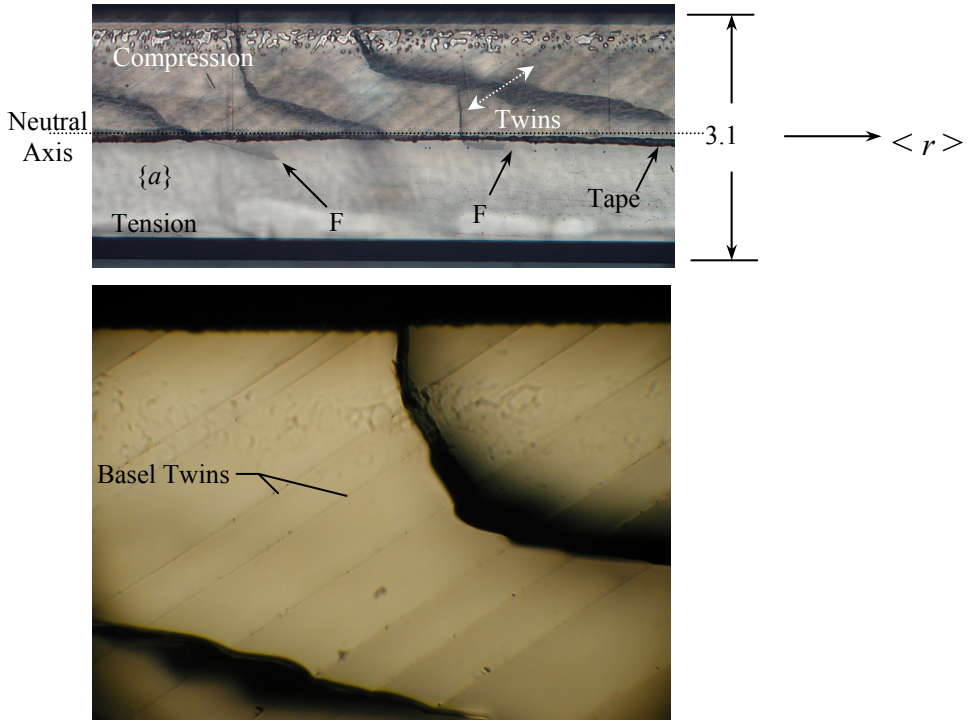

Figure 24.—Side view of an *r*-plane test specimen (R67). The test was interrupted at 1198 MPa during loading in dry nitrogen at 300 MPa/s. Faults leading from the compressive side to just beyond the initial neutral axis of the beam are apparent (arrows marked “F”). Basel plane twins are apparent as the dark shadows running 32° to the neutral axis. Note that the twins align cross the cracks, implying that they occurred first.

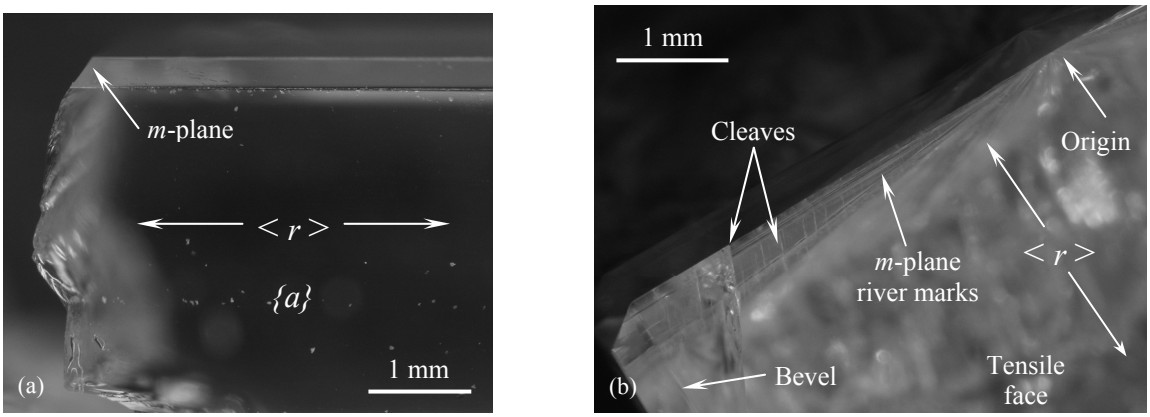

Figure 25.—(a) Side view of an *r*-plane test specimen (R3) showing typical *m*-plane crack extension from the mirror. Failure was from a long surface scratch. (b) Cleaves occurring away from the origin in an *r*-plane test specimen (R10) that failed at 733 MPa. River marks running along the *m*-plane are also apparent by looking through the tensile surface. Bifurcation did not occur along the tensile face.

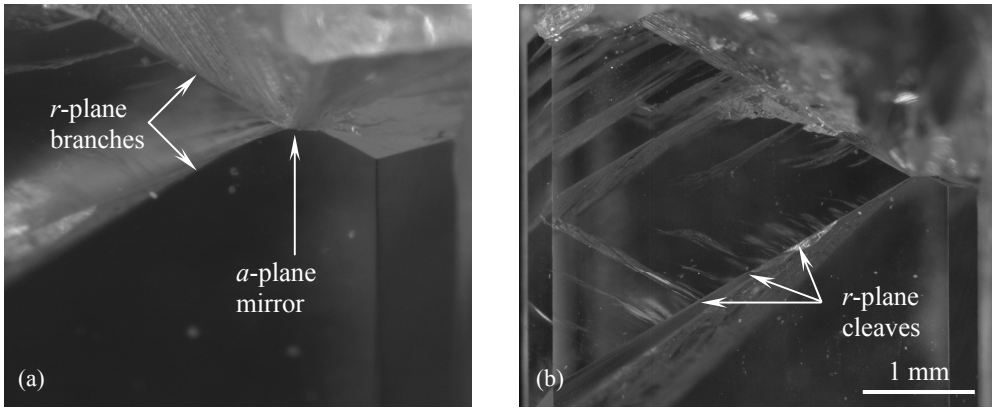

Figure 26.—View of an *a*-plane test specimen (A54) that failed at 1288 MPa: (a) *a*-plane mirror followed by *r*-plane branches, and (b) secondary *r*-plane cleaves that increase in frequency and size with distance from the origin.

The *a*-plane specimens exhibited mirrors on or near the *a*-plane that branched to the *r*-plane. The *r*-plane branches were surrounded by a symmetric series of *r*-plane cracks of increasing frequency and size with increasing failure stress and distance from the origin (Fig. 26). Test specimens failing at ~500 MPa or less usually exhibited no secondary *r*-plane cleaves (though the branches were on the *r*-plane) while specimens failing over ~1 GPa exhibited dozens.

Thus, a specific procedure describing the stages of removal, the feed-rate, grit-sizes and amounts to be removed in each stage is needed for sapphire to avoid the complications described in this section and section 4.2. For purposes of producing a specimen with a ground finish (e.g., 400 grit) the methods described ASTM C 1161 (Ref. 35) might be adequate for test specimens or components with a uniaxial stress state. However, the procedures in ASTM C 1161 impart more damage in the direction parallel to grinding than in the direction perpendicular to grinding. Thus components or test specimens with a multiaxial stress state will fail preferentially along the direction parallel to grinding (Ref. 36). Thus, any polishing needs to remove all of the grinding damage imparted in prior stages.

4.6 Window Strength

Because the windows are larger than the test specimens used to generate the strength and SCG data, the window strength is expected to be lower. The strength of a window at a probability of failure can be estimated from the Weibull scaling equation for a given probability of failure:

$$\sigma_1/\sigma_2 = \left(A_{e2}/A_{e1}\right)^{1/m} \tag{15}$$

where σ_1 and σ_2 are the strengths corresponding to "effective area" A_{e1} and A_{e2}. Because the specimens in this study probably failed from surface connected flaws, the use of an effective area is appropriate. The "effective area" of a simply supported circular plate subjected to a uniform pressure can be calculated from Reference 37

$$Ae \cong \frac{4\pi(1+\nu)}{1+m}\left(\frac{R_s}{R_d}\right)^2\left[\frac{2R_d^2(1+\nu)+R_s^2(1-\nu)}{(3+\nu)(1+3\nu)}\right] \tag{16}$$

within 1 percent for $m > 5$, $\nu > 0.17$ and $R_s/R_d < 0.9$. For uniaxial flexure specimens the effective area is

$$Ae = \left[\frac{1+m(S_i/S_o)}{(m+1)^2}\right]\left[1+\frac{mb}{b+w}\right][b+w]S_o \tag{17}$$

where b is the specimen width, w is the height, and S_i and S_o are the load and support spans respectively. The expected strength of a window for 50 percent probability of failure is summarized in Table 12 for the data sets. It should be noted that the predicted strength based on the *a*-plane data is low due to the poor polishing of the test specimens.

TABLE 12.—ESTIMATED FAST FRACTURE STRENGTH OF A 121 MM DIAMETER, SIMPLY SUPPORTED WINDOW SUBJECTED TO A UNIFORM PRESSURE

Data Set	Test Specimen Characteristic Strength, MPa	Test Specimen Effective Area, mm^2	Window Effective Area, mm^2	Estimated Window Strength for 50 percent Failure, MPa
r-plane, All data, Dry N_2	1135	93.75	2200	843
r-plane, Censored, Dry N_2	1149	90.33	1805	913
r-plane, All data, Water	895[a]	93.75	2335	671
a-plane, Case (2)	1416	109.4	7762	245

[a]Estimated by extrapolation of the slow crack growth curve to the ASTM C1161 rate of 35 MPa/s.

4.7 Choice of Window Orientation

Sapphire windows with *c*-plane and *a*-plane faces have been made, and the choice of window face has usually been based on the size of the window and the size of the sapphire boules available rather than the crystal properties (Ref. 38). However, for high precision applications the *c*-plane is preferred over the *a*- or *m*-planes because it is the zero birefringence orientation. For *c*-orientations, the *a*- and *m*- planes are subjected the principal stress, whereas the *r*-plane is subjected to a normal stress of 71 percent of the principal ($\cos^2 32.4°$), thereby mitigating the effect of the lower *r*-plane fracture toughness in high humidity.

Recent testing of twenty ring-on-ring biaxial strength specimens at room temperature indicated that *c*-face disks are stronger (1053±421 MPa) than *a*-face disks (607±182 MPa) (Ref. 39). The strengths and standard deviations correspond to Weibull moduli of ~3 and ~4 respectively, implying an inconsistent surface finish on disks of both orientations.

4.8 Recommended Values

Because the reported properties of sapphire vary widely, it is recommended that more recent values or values determined for the specific type of sapphire (i.e., crystal systems HEM grade) be used. Based on the preceding sections, the values in Table 13 are recommended. The *m*-plane data is based on reference (Ref. 21) and is similar to the *a*-plane data generated in this work. The *r*-plane values are based on the measurements of HEM sapphire in water. Because design requirements typically use mean strength, the strength corresponding to 50 percent probability of failure for the widow is given.

TABLE 13.—RECOMMENDED PROPERTIES

Plane	A m/s·(MPa√m)$^{-n}$	n	$\overline{\sigma}_f$ MPa (Water)	K_{Ic} MPa√m (Water)	K_{Ic} MPa√m (Dry N_2)	$K_{I\,threshold}$ MPa√m (85 percent RH)
a- or m-plane	1.8×10^{-20}	46 ± 2.5	----	1.94 ± 0.07	2.14	1.65
r-plane	2.81×10^{-14}	21 ± 4	671 ± 71	1.77 ± 0.13	2.47 ± 0.15	----

5. Summary and Conclusions

The fracture toughness, inert flexural strength, and slow crack growth parameters of the *r*- and *a*-planes of HEM sapphire were measured. The fracture toughness in dry nitrogen, K_{Ipb}, was 2.47 ± 0.15 MPa√m and 2.31 ± 0.12 MPa√m for the *r*- and *a*-planes. Fracture toughness measured in water via the operational procedure in ASTM C1421 was significantly lower, 1.95 ± 0.03 MPa√m, 1.94 ± 0.07 and 1.77 ± 0.13 MPa√m for the *a*- , *m*- and *r*-planes. The mean uniaxial inert strength in dry nitrogen was 1085 ± 127 MPa for the *r*-plane and 1255 ± 547 MPa for the *a*-plane. The measured strengths are a result of the polishing of the material rather than an inherent material property. The power law slow crack growth exponent was $n = 21 \pm 4$ for the *r*-plane and $n \geq 31$ for the *a*-plane. The *r*-plane of HEM sapphire is relatively susceptible to stress corrosion induced slow crack growth in water. Data for HEM *a*-plane sapphire tested in water agreed with recent *m*-plane data sets for 85 percent RH and dry nitrogen. The published literature and the data reported herein indicate that the fracture toughness and SCG resistance of the *r*-plane of sapphire have improved since the 1960s, with the stress intensity levels nearly doubling.

Interferences to testing due to test specimen preparation included the frequent occurrence of a “short” finish, occasional and severe chips on bevels, and an asymmetric bevel polishing in which one bevel retained severe grinding damage. A consistent, well defined method for preparation of sapphire is needed, even if consistency is gained at the sacrifice if absolute strength. This would impart higher component reliability despite the sacrifice in absolute strength of the component.

The strength difference between the two planes tested is due to the difference in specimen preparation rather than the difference in the stress corrosion properties associated with the specific crystallographic planes. If the strength scatter (i.e., the low Weibull modulus) associated with the *a*-plane material can be eliminated either by more consistent polishing or proof testing, a better estimate of the *a*-plane slow crack growth parameters could be made from strength data.

In order to minimize twinning in the failure process and insure that SCG is the dominant mechanism in dynamic fatigue testing, the stress rates should be relatively low, and water should be used. Testing circular disks via pressure loading might improve data quality. Manufacturing of disk is simpler and the issues associated with bevels and contact stresses are reduced. Further, pressurized disks provide a better analogy to an actual window and extrapolation of the test specimen characteristic strength to that of the component is lessened. Unfortunately, an ASTM standard for such testing does not exist. However, a standard for concentric ring testing, which produces a similar stress state, has been developed (Refs. 40 and 41).

Recommendations

Determination of the threshold stress intensity for the *a-, m-,* and *r*-planes for HEM sapphire in air and water is recommended.

Appendix—Summary Reports on Testing

TABLE A1.—ELASTIC MODULUS OF SAPPHIRE TEST SPECIMENS

	Length mm	Height mm	Width mm	Mass g	Flexural Frequency (Hz)	Density g/cc	Poisson's Ratio ν	E GPa	Corrected E GPa
(No Bevel on KA-, KM-, or KR- specimens)									
KA-21	51.10	3.023	4.066	2.5010	12137	3.982	0.26	424.4	424.4
KA-22	51.07	3.028	4.060	2.4968	12169	3.977	0.26	423.8	423.8
KA-23	51.10	3.024	4.080	2.5121	12179	3.985	0.26	427.4	427.4
KA-24	51.06	3.013	4.077	2.4933	12097	3.975	0.26	422.3	422.3
KA-25	51.07	3.025	4.079	2.5094	12173	3.982	0.26	425.4	425.4
A56	51.34	3.100	4.125	2.5946	12256	3.952	0.26	416.6	433.1
A57	51.34	3.099	4.114	2.5887	12250	3.956	0.26	416.9	433.4
A58	51.33	3.100	4.125	2.5972	12252	3.957	0.26	416.5	433.0
A59	51.34	3.101	4.110	2.5897	12250	3.958	0.26	416.4	432.9
A60	51.35	3.100	4.121	2.5964	12247	3.958	0.26	416.9	433.4
A-46	51.35	3.100	4.112	2.5901	12246	3.957	0.26	416.8	433.2
A-55	51.34	3.099	4.116	2.5865	12258	3.950	0.26	416.8	433.2
								a-plane average = 430 ± 5	
KM-21	51.07	3.052	4.053	2.5088	12246	3.971	0.26	422.0	422.0
KM-22	51.04	3.042	4.040	2.4960	12228	3.979	0.26	423.3	423.3
KM-23	51.03	3.052	4.042	2.5022	12242	3.975	0.26	420.8	420.8
KM-24	51.05	3.047	4.055	2.5069	12230	3.974	0.26	421.9	421.9
KM-25	51.05	3.047	4.053	2.5050	12241	3.973	0.26	422.6	422.6
MU-1	51.58	3.083	4.088	2.565	12036	3.946	0.26	413.0	429.3
MU-2	51.49	3.083	4.086	2.5655	12046	3.955	0.26	411.9	428.1
MU-3	51.33	3.095	4.086	2.5654	12161	3.952	0.26	411.2	427.4
MU-4	51.53	3.082	4.075	2.5612	12058	3.958	0.26	414.4	430.8
MU-5	51.54	3.085	4.08	2.5576	12110	3.943	0.26	416.0	432.4
MU-6	51.55	3.087	4.086	2.5639	12075	3.943	0.26	413.4	429.8
								m-plane average = 426 ± 4	

TABLE A1 (CONTINUED).—ELASTIC MODULUS OF SAPPHIRE TEST SPECIMENS

	Length mm	Height mm	Width mm	Mass g	Flexural Frequency (Hz)	Density g/cc	Poisson's Ratio ν	E GPa	Corrected E GPa
(No Bevel on KA-, KM-, or KR- specimens)									
KR-21	51.00	3.035	4.074	2.5160	10973	3.990	0.26	342.3	342.3
KR-22	51.07	3.039	4.063	2.5112	10973	3.982	0.26	342.6	342.6
KR-23	51.01	3.034	4.062	2.5099	10973	3.993	0.26	343.0	343.0
KR-24	51.02	3.035	4.063	2.5108	10983	3.991	0.26	343.5	343.5
KR-25	51.09	3.039	4.065	2.5138	10979	3.983	0.26	343.6	343.6
RU-1	53.21	3.065	4.099	2.6352	10092	3.942	0.26	331.8	344.9
RU-2	53.39	3.072	4.097	2.6471	10027	3.939	0.26	330.3	343.3
RU-3	53.32	3.069	4.095	2.6474	10073	3.951	0.26	333.2	346.4
RU-4	53.19	3.073	4.099	2.6366	10106	3.935	0.26	330.0	343.1
RU-5	53.34	3.075	4.099	2.641	10062	3.928	0.26	329.8	342.8
R56	51.32	3.058	4.091	2.5384	10856	3.954	0.26	335.3	348.5
R57	51.28	3.057	4.093	2.5383	10847	3.956	0.26	334.2	347.4
R58	51.3	3.066	4.094	2.5477	10883	3.956	0.26	335.0	348.3
R59	51.27	3.070	4.096	2.5502	10895	3.956	0.26	334.0	347.2
R60	51.31	3.058	4.094	2.5394	10845	3.953	0.26	334.3	347.5
								***r*-plane average = 345 ± 2**	

TABLE A2.—HARDNESS OF SAPPHIRE TEST SPECIMENS. TEN TESTS WERE RUN PER CONDITION.

Orientation	Knoop HK0.1/15	Vickers HV0.1/15	Vickers HV0.5/15
c-plane diagonal parallel to the *a*-axis	19.6 ± 1.3	20.6 ± 1.2	19.6 ± 1.3
a-plane diagonal parallel to the *m*-axis	19.0 ± 1.0	**	
a-plane diagonal parallel to the *r*-axis	18.0 ± 1.1	**	
m-plane diagonal parallel to the a-axis	21.7 ± 0.9	**	
Tensile face of *r*-plane specimen Diagonal parallel to *r*-axis	21.0 ± 1.3	**	

** For 0.1 kg load, spherically shaped indentations formed. For 0.1 kg, heavy cracking occurred.

TABLE A3.—SUMMARY OF *a*-PLANE VB FRACTURE TOUGHNESS RESULTS FOR TESTING IN AIR OR WATER.
GRAYED VALUES EXCEED THE SPECIFICATIONS OF ASTM C1421. STRUCK-THROUGH VALUES ARE INVALID.

Tare = 1.631 N ***So*** **=** 19.951 mm Stroke
Si **=** 9.977 Rate = 0.20 mm/min

Bevel Correction = 1.029

Spec Number	*B* mm	*W* mm	Notch Width	Plane Offset mm	Normalized Notch Parameters: α_0	α_{11}	α_{12}	α_1	Load *P* N	Test Stability, Comments	K_{Ivb} MPa√m
					Air:						
A56	3.100	4.125	0.224	0.000	0.199	0.952	0.948	0.950	23.05	Overload	~~2.50~~[5]
A57	3.099	4.114	0.256	0.044	0.190	0.942	0.949	0.946	18.16	Yes, corrected Y*	1.96
A58	3.100	4.125	0.242	0.025	0.198	0.953	0.945	0.949	17.91	Yes, corrected Y*	1.96
A59	3.101	4.110	0.296	0.070	0.195	0.944	0.948	0.946	17.13	Yes, corrected Y*	1.88
A60	3.100	4.121	0.293	0.094	0.189	0.949	0.937	0.943	17.08	Yes, corrected Y*	1.84
KA-III-1	3.019	4.081	0.292	0.005	0.190	0.953	0.960	0.957	21.64	Yes	2.37
KA-III-2	3.032	4.062	0.293	0.007	0.198	0.970	0.958	0.964	15.79	Yes, corrected Y*	2.09
KA-III-3	3.025	4.086	0.288	0	0.186	0.949	0.964	0.956	21.58	Yes	2.33
											Average = 2.06 ± 0.21
					Water:						
A-II-2	3.052	3.995	.321	0.096	0.206	0.987	0.988	0.987	17.68	No	~~2.19~~
A-II-4	3.048	3.995	.327	0.102	0.207	0.981	0.983	0.982	17.25	Yes	2.07
KA-III-7	3.014	4.085	0.289	0.005	0.179	0.943	0.940	0.942	17.55	Yes, long precrack	1.90
KA-III-8	3.016	4.082	0.293	0.013	0.185	0.950	0.956	0.953	17.74	Yes	1.95
KA-III-9	3.025	4.058	0.287	0	0.193	0.965	0.957	0.961	17.44	Yes	1.97
KA-III-10	3.032	4.081	0.288	0	0.195	0.966	0.959	0.963	--------	Broken	
KA-III-11	3.038	4.088	0.292	0	0.191	0.957	0.963	0.960	19.060	Yes, tilted precrack	~~2.09~~
KA-III-12	3.018	4.073	0.298	0.02	0.185	0.952	0.951	0.951	17.890	Yes	1.96
KA-III-13	3.031	4.062	0.289	0.04	0.186	0.959	0.962	0.960	17.940	Yes	1.98
KA-III-14	3.032	4.080	0.284	0.035	0.192	0.963	0.957	0.960	17.600	Yes	1.96
KA-III-15	3.024	4.075	0.288	0	0.188	0.959	0.965	0.962	16.430	Yes, curved front	~~1.93~~
											Average = 1.95 ± 0.03

TABLE A4.—SUMMARY OF *m*-PLANE VB FRACTURE TOUGHNESS RESULTS FOR TESTING IN AIR OR WATER. GRAYED VALUES EXCEEDED THE SPECIFICATION IN ASTM C1421. STRUCK-THROUGH VALUES ARE INVALID.

Tare = 1.631 N ***So*** **=** 19.951 mm Stroke

Si **=** 9.977 Rate = 0.20 mm/min

Bevel Correction = 1.029

Specimen Number	*B* mm	*W* mm	Notch Width	Plane Offset mm	Normalized Notch Parameters: α_0	α_{11}	α_{12}	α_1	Load *P* N	Test Stability, Comments	K_{Ivb} MPa√m
						Water:					
M-II-4	3.086	4.083	0.309	0.078	0.205	0.964	0.954	0.959	16.65	Semi-stable	1.98
KM-III-5	3.047	4.058	0.280	0.007	0.185	0.959	0.969	0.964	21.68	Yes, tilted	~~2.36~~[5]
KM-III-6	3.045	4.069	0.285	0.007	0.192	0.965	0.968	0.966	----	Broken	
KM-III-7	3.052	4.038	0.288	0.013	0.191	0.970	0.966	0.968	15.23	Yes, long precrack	1.82
KM-III-8	3.039	4.070	0.291	0.009	0.189	0.962	0.967	0.964	18.51	Yes, tilted	~~2.05~~
KM-III-9	3.046	4.051	0.291	0	0.185	0.966	0.965	0.966	17.22	Yes, long precrack	1.91
KM-III-10	3.049	4.074	0.288	0.028	0.196	0.969	0.975	0.972	17.49	Yes	1.97
KM-III-11	3.044	4.046	0.281	0.005	0.191	0.972	0.966	0.969	19.70	Yes, tilted	~~2.20~~
KM-III-12	3.046	4.043	0.285	0	0.190	0.975	0.964	0.969	17.02	Yes, long precrack	1.92
KM-III-13	3.041	4.070	0.289	0	0.195	0.967	0.962	0.965	17.32	Yes	1.95
KM-III-14	3.052	4.080	0.282	0	0.196	0.966	0.967	0.966	20.65	Yes, tilted	~~2.29~~
KM-III-15	3.045	4.067	0.286	0	0.193	0.968	0.961	0.965	16.92	Yes	1.90
KM-III-16	3.048	4.055	0.282	0	0.188	0.968	0.964	0.966	18.36	Yes	2.04
KM-III-17	3.046	4.076	0.280	0	0.192	0.965	0.967	0.966	18.11	Yes	2.01

Average = 1.94 ± 0.07

[5]Strikethrough values were not used in estimation of averages.

TABLE A5.—SUMMARY OF *r*-PLANE VB FRACTURE TOUGHNESS RESULTS FOR TESTING IN AIR OR WATER. GRAYED VALUES EXCEEDED THE SPECIFICATION IN ASTM C1421. STRUCK-THROUGH VALUES ARE INVALID.

				Tare =	1.631	N	***So*** **=**	19.951	mm	Stroke		
				Bevel Correction =	1.029		***Si*** **=**	9.977		Rate =	0.20	mm/min
			Notch	**Plane**	**Normalized Notch Parameters:**					**Load**	**Test**	
Specimen	***B***	***W***	**Width**	**Offset**	α_0	α_{11}	α_{12}	α_1		***P***	**Stability,**	K_{Ivb}
Number	**mm**	**mm**		**mm**						**N**	**Comments**	**MPa√m**
						Air:						
R58	3.066	4.094	0.498	0.157	0.167	0.939	0.938	0.938		18.97	Yes, corrected Y*	1.98
R59	3.070	4.096	0.475	0.172	0.150	0.938	0.947	0.942		21.9	No	~~2.19~~[6]
R60	3.058	4.094	0.516	0.206	0.148	0.942	0.946	0.944		19.12	Yes, corrected Y*	1.94
						Water:						
R-II-1	2.936	4.012	0.314	0.114	0.183	0.954	0.947	0.951		9.14	Yes	1.82
R-II-2	2.940	4.010	0.322	0.092	0.192	0.948	0.950	0.949		14.20	Yes	1.80
R-II-3	2.939	4.011	0.350	0.093	0.182	0.953	0.950	0.952		16.02	Yes	1.87
R-II-4	2.938	4.009	0.326	0.088	0.181	0.952	0.950	0.951		14.50	Yes	1.70
R-II-5	2.936	4.013	0.321	0.121	0.195	0.952	0.956	0.954		16.08	Yes	1.93
KR-III-3	3.040	4.065	0.293	0	0.194	0.959	0.955	0.957		17.77	Yes, large step	1.99
KR-III-6	3.043	4.069	0.285	0	0.181	0.958	0.974	0.966		13.47	Yes	1.51
KR-III-12	3.041	4.060	0.294	0.009	0.194	0.971	0.962	0.966		8.40	Yes, long precrack	1.73
KR-III-13	3.033	4.059	0.280	0	0.188	0.967	0.970	0.968		14.86	Yes, long precrack	1.70
KR-III-14	3.034	4.056	0.290	0	0.191	0.964	0.968	0.966		-------	Broken	
KR-III-15	3.032	4.063	0.292	0	0.190	0.967	0.966	0.966		17.82	Yes, tilted precrack	~~1.99~~
KR-III-16	3.036	4.055	0.285	0	0.190	0.969	0.959	0.964		15.07	Yes	1.71
KR-III-17	3.035	4.057	0.289	0	0.194	0.970	0.965	0.968		15.17	Yes	1.74
KR-III-18	3.042	4.069	0.287	0	0.190	0.960	0.964	0.962		16.54	Yes	1.85
KR-III-19	3.043	4.047	0.291	0	0.192	0.964	0.968	0.966		12.23	Yes, slow loading	~~1.42~~
KR-III-20	3.043	4.063	0.290	0.006	0.190	0.966	0.960	0.963		18.15	Yes, tilted precrack	~~2.02~~
											Average = 1.77 ± 0.13	

[6]Strikethrough values were not used in estimation of averages.

TABLE A6.—SUMMARY OF *r*-PLANE PB FRACTURE TOUGHNESS RESULTS FOR TESTING IN DRY NITROGEN AND SILICONE OIL. GRAYED VALUES EXCEEDED THE SPECIFICATION IN ASTM C1421. STRUCK-THROUGH VALUES ARE INVALID.

Tare = 1.631 N ***So*** **=** 19.951 mm Stroke

Si **=** 9.977 Rate = 0.20 mm/min

Bevel Correction = 1.029

		Crack Length:									**Load**		
Specimen Number	**Indent Load**	***a1*** **mm**	***a2*** **mm**	***a3*** **Mm**	**Δ*a1*** **%**	**Δ*a2*** **%**	**Δ*a3*** **%**	***a/W***	***B*** **mm**	***W*** **mm**	***P*** **N**	**Test Stability**	**K_{Ipb} MPa√m**
						Dry N2:							
R56	5 x 3 kg	2.502	2.55	2.355	1.3	3.3	-4.6	0.60	3.058	4.091	46.72	Yes	2.48
R57	5 x 3 kg	2.47	2.37	2.193	5.4	1.1	-6.5	0.57	3.057	4.093	51.85	Yes	2.45
R58	5 x 3 kg	1.932	2.044	2.063	-4.0	1.5	2.5	0.49	3.066	4.094	65.53	Yes	2.35
R59	5 x 4 kg	1.743	1.642	1.512	6.8	0.6	-7.4	0.40	3.070	4.096	97.3	Yes	2.67
R60	5 x 4 kg	2.196	2.135	2.109	2.3	-0.5	-1.8	0.52	3.058	4.094	64.89	Yes	2.58
RU4	5 x 5 kg	2.612	2.587	2.501	1.8	0.8	-2.6	0.63	3.073	4.099	41.35	Yes	~~2.39~~[7]
RU5	5 x 5 kg	2.076	2.024	1.959	2.8	0.2	-3.0	0.49	3.075	4.099	63.20	Yes	2.27
						Oil:							
R57-2	5 x 4 kg	2.581	2.592	2.532	0.5	0.9	-1.4	0.63	3.057	4.093	47.28	Yes	~~2.76~~
R58-2	5 x 4 kg	2.857	2.866	2.819	0.3	0.7	-1.0	0.70	3.066	4.094	32.58	Yes	~~2.58~~
R59-2	5 x 4 kg	3.552	3.532	3.512	0.6	0.0	-0.6	0.86	3.070	4.096	12.28	Yes	~~2.47~~
R60-2	5 x 4 kg	2.843	2.872	2.932	-1.4	-0.4	1.7	0.70	3.058	4.094	31.99	Yes	~~2.65~~
RU1	5 x 5 kg	2.820	2.881	2.911	-1.8	0.4	1.4	0.70	3.075	4.099	30.97	Yes	~~2.51~~
RU2	5 x 5 kg	2.981	3.091	3.105	-2.5	1.0	1.5	0.75	3.075	4.099	22.45	Yes	~~2.31~~

[7]Strikethrough values were not used in estimation of averages.

TABLE A7.—SUMMARY OF *a*-PLANE SEPB FRACTURE TOUGHNESS RESULTS FOR TESTING IN DRY NITROGEN AND SILICONE OIL. GRAYED VALUES EXCEEDED THE SPECIFICATION IN ASTM C1421. STRUCK OUT VALUES ARE INVALID.

Tare = 1.631 N ***So*** **=** 19.951 mm Stroke

Si **=** 9.977 Rate = 0.20 mm/min

Bevel Correction = 1.029

		Crack Length:									**Load**		
Specimen Number	**Indent Load**	***a1*** **mm**	***a2*** **mm**	***a3*** **mm**	**Δ*a1*** **%**	**Δ*a2*** **%**	**Δ*a3*** **%**	***a/W***	***B*** **mm**	***W*** **mm**	***P*** **N**	**Test Stability**	**KIpb MPa√m**
						Dry N2:							
A56	5 x 3 kg	2.849	2.758	2.755	2.2	-1.1	-1.2	0.68	3.100	4.125	36.87	Yes	~~2.60~~[8]
A57	5 x 5 kg	2.307	2.001	1.676	15.7	0.3	-16.0	0.48	3.099	4.114	58.07	Yes	~~2.01~~
A58	5 x 5 kg	2.046	2.345	2.571	-11.8	1.0	10.8	0.56	3.100	4.125	49.69	Yes	~~2.21~~
A59	5 x 5 kg	2.277	2.227	2.2	1.9	-0.3	-1.6	0.54	3.100	4.125	53.27	Yes	2.20
A60	5 x 5 kg	2.207	2.256	2.288	-1.9	0.3	1.7	0.55	3.100	4.121	56.79	Yes	2.38
AU1	5 x 5 kg	2.302	2.334	2.302	-0.5	0.9	-0.5	0.56	3.104	4.122	54.91	Yes	2.42
AU2	5 x 5 kg	2.148	2.348	2.458	-7.3	1.3	6.0	0.56	3.103	4.126	45.89	Yes	2.17
AU3	5 x 5 kg	2.009	2.063	2.077	-2.0	0.7	1.3	0.50	3.111	4.113	65.12	Yes	2.33
AU4	5 x 5 kg	2.108	2.053	1.927	3.9	1.2	-5.0	0.49	3.107	4.111	60.78	Yes	2.16
AU5	5 x 5 kg	2.082	1.979	1.887	5.0	-0.2	-4.8	0.48	3.106	4.115	64.19	Yes	2.19
						Oil:							
A56-2	5 x 4 kg	2.516	2.536	2.521	-0.3	0.5	-0.1	0.61	3.100	4.125	45.40		2.43
A58-2	5 x 4 kg	2.232	2.332	2.313	-2.6	1.7	0.9	0.56	3.100	4.125	57.18		2.47
A59-2	5 x 4 kg	2.55	2.582	2.577	-0.8	0.5	0.3	0.63	3.101	4.110	43.7		~~2.48~~
A60-2	5 x 4 kg	2.06	2.125	2.161	-2.6	0.5	2.2	0.51	3.100	4.121	63.96		2.40

[8]Strikethrough values were not used in estimation of averages.

TABLE A8.—SUMMARY OF *r*-PLANE FRACTURE STRENGTH
FOR TESTING IN WATER AND DRY NITROGEN

Sapphire	**Load Span:**	20.176	**mm**	
r-plane	**Support Span:**	40.292	**mm**	
	Tare:	2.26	**N**	
Instron 8562, 5000N	**Environment:**	Distilled, Deionized Water or 99.98% Dry Nitrogen		
	Bevel Correction:	1.029	**%**	
	Preload:	300	**N**	

Specimen ID	Loading Rate N/s	Stressing Rate MPa/s	Width *b* mm	Height *w* mm	Failure Load N	Fracture Strength MPa
			Distilled Water			
R1	2.4	1.884785	4.098	3.062	919.5	744.9
R2	2.45	1.926872	4.092	3.062	923.1	748.9
R3		1.923550	4.096	3.063	423.3	**343.8**
R4		1.932943	4.089	3.058	1054.0	857.5
R5		1.930534	4.084	3.062	1162.0	944.0
R6		1.936374	4.096	3.053	1091.0	889.1
R7		1.918775	4.086	3.071	1130.0	912.5
R8		1.914016	4.096	3.071	999.3	805.1
R9		1.925939	4.091	3.063	1170.0	948.2
R10		1.924541	4.087	3.066	903.9	732.5
R11		1.917383	4.092	3.070	1121.0	904.6
R12		1.914808	4.091	3.072	1026.0	826.9
R13		1.943805	4.077	3.054	1097.0	897.4
R14		1.930139	4.092	3.059	984.1	799.6
R15		1.921556	4.093	3.066	1063.0	859.7
R45		1.916142	4.098	3.069	1115	899.1
R61		1.913102	4.092	3.073	679.3	**547.6**
R63		1.914036	4.094	3.072	1051	846.7
R16	0.245	0.191857	4.089	3.070	929.0	750.4
R17		0.191758	4.088	3.071	913.9	737.9
R18		0.192694	4.092	3.062	485.8	**395.0**
R19		0.192434	4.091	3.065	921.7	746.8
R20		0.193194	4.088	3.059	891.4	725.1
R21	0.0245	0.019248	4.091	3.064	754.3	611.6
R22		0.019186	4.091	3.069	779.2	629.7
R23		0.019244	4.088	3.066	867.4	702.9
R24		0.019459	4.088	3.049	736.2	603.5
R25		0.019269	4.092	3.062	858.4	696.5

TABLE A8 (CONTINUED).—SUMMARY OF *r*-PLANE FRACTURE STRENGTH FOR TESTING IN WATER AND DRY NITROGEN

Sapphire	**Load Span:**	20.176	**mm**
Rhombohedral	**Support Span:**	40.292	**mm**
	Tare:	2.26	**N**
Instron 8562, 5000N	**Environment:**	Distilled, Deionized Water or 99.98% Dry Nitrogen	
	Bevel Correction:	1.029	**%**
	Preload	300	**N**

Specimen ID	Loading Rate N/s	Stressing Rate MPa/s	Width *b* mm	Height *w* mm	Failure Load N	Fracture Strength MPa
			Distilled Water			
R26	0.00245	0.001922	4.092	3.066	526.4	**426.7**
R27		0.001920	4.094	3.067	661.2	534.9
R28		0.001934	4.093	3.056	754.3	614.5
R29		0.001937	4.094	3.053	745.8	608.7
R30		0.001940	4.092	3.052	770.3	629.3
R31		0.001934	4.095	3.055	780.3	635.8
R32		0.001926	4.089	3.064	793.4	643.5
R33		0.001923	4.089	3.066	760.4	616.1
R34		0.001924	4.088	3.066	825.4	668.8
R35		0.001921	4.094	3.066	743.7	601.8
R36		0.001928	4.087	3.063	636.8	517.4
R37		0.001935	4.088	3.057	720.6	587.5
R38		0.001932	4.091	3.058	718.8	585.2
R39		0.001939	4.093	3.052	633.6	517.9
R40		0.001930	4.088	3.061	680.3	553.4
R69		0.001930	4.093	3.060	703.1	571.7
R44	30	23.694968	4.096	3.054	1246	1014.5
			Dry Nitrogen			
R46	385	301.0	4.096	3.070	1453	1170.83
R47		303.4	4.094	3.058	1231	999.96
R48		304.5	4.090	3.055	1301	1060.54
R49		304.4	4.091	3.055	934.2	**761.87**
R50		301.3	4.092	3.070	1529	1232.93
R51		303.9	4.086	3.059	1342	1091.98
R52		303.4	4.092	3.059	1386	1125.70
R53		304.4	4.093	3.054	1448	1179.93
R54		301.4	4.093	3.069	1451	1170.84
R55		301.4	4.095	3.068	1288	1039.35
R64		301.9	4.097	3.065	1373	1109.81
R65		301.4	4.097	3.068	1449	1168.99
R66		300.3	4.097	3.073	1179	947.99
R67		303.0	4.087	3.063	1198	971.91
R68		303.1	4.089	3.062	1531	1241.91

TABLE A9.—SUMMARY OF *a*-PLANE FRACTURE STRENGTH FOR TESTING IN WATER AND DRY NITROGEN

Sapphire	**Load Span:**	20.176	**mm**
a-plane	**Support Span:**	40.292	**mm**
	Tare:	2.26	**N**
Instron 8562, 5000N	**Environment:**	Distilled, Deionized Water or 99.98% Dry Nitrogen	
	Bevel Correction:	1.029	**%**
	Preload	300 to 500	**N**

Specimen ID	Loading Rate N/s	Stressing Rate MPa/s	Width *b* mm	Height *w* mm	Failure Load N	Fracture Strength MPa
			Distilled Water			
A1	30	22.74	4.128	3.106	478.4	374.9
A2		22.76	4.130	3.104	2303.0	1799.6
A3		22.74	4.130	3.105	1930.0	1507.4
A4		22.86	4.112	3.104	1084.0	851.6
A5		22.79	4.121	3.105	1391.0	1089.3
A7		22.83	4.118	3.103	1351.0	1059.7
A8		22.70	4.129	3.108	1754.0	1367.4
A9		22.72	4.122	3.110	728.1	569.0
A10		22.81	4.118	3.105	921.3	722.6
A12		22.83	4.116	3.104	1661.0	1302.7
A13		22.83	4.121	3.102	2077.0	1628.1
A14		22.77	4.128	3.104	1521.0	1189.7
A17		22.75	4.128	3.105	369.2	289.8
A18		22.82	4.119	3.103	1764.0	1382.8
A19		22.74	4.126	3.106	954.6	746.4
A47		22.73	4.133	3.105	1477.0	1153.0
A48		22.83	4.120	3.103	2316.0	1815.3
A49		22.79	4.129	3.102	679.6	533.1
A50		22.88	4.112	3.102	1393.0	1095.0
A15	0.3	0.228442	4.110	3.105	597.3	469.8
A16		0.229263	4.108	3.100	1242.0	978.4
A21	0.03	0.022844	4.120	3.101	1383.0	1085.4
A22		0.022910	4.115	3.099	1469.0	1156.1
A23		196.33413	4.125	3.101	499.5	392.7
A24		0.022905	4.112	3.100	1613.0	1269.0
A25		0.022917	4.114	3.099	671.0	529.2
A26	0.00245	0.001870	4.116	3.099	1657.0	1303.3

TABLE A9 (CONTINUED).—SUMMARY OF *a*-PLANE FRACTURE STRENGTH FOR TESTING IN WATER AND DRY NITROGEN

Sapphire	**Load Span:**	20.176	**mm**
a-plane	**Support Span:**	40.292	**mm**
	Tare:	2.26	**N**
Instron 8562, 5000N	**Environment:**	Distilled, Deionized Water or 99.98% Dry Nitrogen	
	Bevel Correction:	1.029	**%**
	Preload	300 to 500	**N**

Specimen ID	Loading Rate N/s	Stressing Rate MPa/s	Width *b* mm	Height *w* mm	Failure Load N	Fracture Strength MPa
			Distilled Water			
A27	0.003	0.002291	4.121	3.096	732.8	577.7
A28		0.002289	4.119	3.099	720.4	567.3
A29		0.002294	4.110	3.099	629.3	496.9
A30		0.002280	4.124	3.103	1575	1233.7
A31		0.002285	4.116	3.103	1587	1245.4
A32		176.999	4.121	3.100	449.3	354.0
A33		0.002285	4.115	3.103	1709	1341.4
A34		0.002294	4.110	3.099	713.5	563.1
A35		0.002281	4.126	3.101	1291	1011.8
A36		0.002286	4.111	3.104	638	501.9
A37		0.002287	4.116	3.101	697	548.5
A38		0.002283	4.115	3.104	1561	1224.4
A39		0.002283	4.115	3.104	1121	879.8
A40		0.002291	4.115	3.099	879.8	693.1
A51		0.002282	4.118	3.104	489.5	384.9
A66		0.002269	4.128	3.109	1064	830.0
A68		0.002284	4.110	3.105	640.8	503.9
A69		0.002276	4.123	3.106	1213	948.8
A70		0.002278	4.126	3.104	491.8	386.1
A71		0.002281	4.117	3.105	1136	890.7
			Dry Nitrogen			
A41	385	292.3570	4.126	3.104	1923	1504.4
A42		292.8184	4.119	3.104	1793	1405.0
A43		292.1920	4.127	3.104	2792	2182.2
A44		292.3683	4.128	3.103	2285	1787.3
A45		291.9573	4.125	3.106	1882	1470.3
A61		293.1241	4.124	3.100	2224	1744.1
A62		293.5635	4.117	3.101	1711	1344.2
A63		292.7931	4.126	3.101	1846	1446.4
A64		292.9472	4.123	3.102	2257	1768.9
A65		292.6776	4.117	3.105	928.9	728.4
A52		291.9126	4.119	3.109	758.3	593.4
A53		292.5465	4.122	3.104	676.6	530.8
A54		292.7939	4.122	3.103	1643	1287.5
A72		292.5355	4.119	3.105	861.9	675.7
A73		292.6653	4.119	3.105	463.4	364.2

References

1. MIL-PRF-13830B "Performance Specifications for Optical Components for Fire Control Instruments: General Specifications Governing The Manufacturing, Assembly and Inspection Of," January 9, 1997.
2. ASTM C 1259-94 "Standard Test Method for Dynamic Young's Modulus, Shear Modulus, and Poisson's Ratio for Advanced Ceramics by Impulse Excitation of Vibration," American Society for Testing and Materials *Annual Book of Standards*, Vol. 15.01, pp. 336–384, 1995.
3. W.E. Teft "Elastic Constants of Synthetic Crystal Corundum," *J. Res. Nat. Bureau Standards,* 70A, (4) pp. 277–280, 1966.
4. ASTM C 1421-99, "Standard Test Method for Fracture Toughness of Advanced Ceramics," American Society for Testing Materials *Annual Book of Standards*, Vol. 15.01, ASTM, West Conshohocken, PA, 2000.
5. J.A. Salem, L. Ghosn, M.G. Jenkins and G.D. Quinn, "Stress Intensity Factor Coefficients For Chevron-Notched Flexure Specimens and A Comparison Fracture Toughness Methods," *Ceramic Engineering and Science Proceedings*, Vol. 20, No. 3, pp. 503–512 (1999).
6. Inspections performed at Brookhaven National Laboratory by Robert Polvani and David Black of the National Institute for Standards and Technology, Gaithersburg, MD, 2000.
7. ASTM C 1368-97, "Standard Test Method for Determination of Slow Crack Growth Parameters of Advanced Ceramics by Constant Stress-Rate Flexural Testing," American Society for Testing and Materials *Annual Book of Standards*, Vol. 15.01, pp. 616–624, 2000.
8. S.G. Ivanova F. Schmidt, C.P. Khattak and D. Harris, "Use of Grafoil in Mechanical Testing of Sapphire at Elevated Temperatures," Proceeding of SPIE, Vol. 4102, Inorganic Optical Materials II, pp. 37–42, 2000.
9. J.A. Salem, and M.G. Jenkins, "The Effect Of Stress Rate On Slow Crack Growth Parameters," pp. 213–227 in *Fracture Resistance Testing of Monolithic and Composite Brittle Materials,*" *ASTM STP 1409*, J.A. Salem, G.D. Quinn, and M.G. Jenkins, Eds., American Society for Testing and Materials, West Conshohocken, PA, 2001.
10. J.E. Ritter, "Engineering Design and Fatigue Failure of Brittle Materials," in *Fracture Mechanics of Ceramics*, Vol. 4, R.C. Bradt, D.P.H. Hasselman, and F.F. Lange, Eds., Plenum Publishing Co., NY, 1978, pp. 661–686.
11. J.A. Salem and A. Weaver, "Estimation and Simulation of Slow Crack Growth Parameters from Constant Stress Rate Data," pp. 579–596 in Fracture Mechanics of Ceramics: Active Materials, Nanoscale Materials, Composites, Glass, and Fundamentals, R.C. Bradt, D. Munz, M. Sakai, and K. White, eds., Springer (2005).
12. R. Szilard, p. 628 in *Theory and Analysis of Plates, Classical and Numerical Methods*, Prentice-Hall, Englewood Cliffs, NJ, 1974.
13. S.P. Timoshenko, and S. Woinowsky-Krieger, p. 72 in *Theory of Plates and Shells,* 2^{ed}, McGraw-Hill, New York, NY, 1959.
14. J.A. Salem and M.G. Jenkins, "Biaxial Strength Testing of Isotropic and Anisotropic Monoliths," pp. 13–25 in Multiaxial Fatigue and Deformation: Testing and Prediction, ASTM STP 1387, S. Kalluri and P.J. Bonacuse, Eds., American Society for Testing and Materials, Philadelphia, Pennsylvania (2000).
15. J.A. Salem, J. Manderscheid and M. Jenkins "Multiaxial Strength Testing of Brittle Single Crystals," Ceramic Engineering and Science Proceedings, Vol. 21, No. 3, pp. 83–90, 2000.
16. J.A. Salem and J.M. Manderscheid, "Stresses in a Thin, Aeolotropic Circular Plate Subjected to Uniform Lateral Load," J. Physics D: Applied Physics, 36, (November, 2003) 2730–2737.
17. S.M. Wiederhorn and R.F. Krause, Jr., "Crack Growth in Sapphire," *Ceram. Eng. Sci. Proc.*, vol. 23, issue 3A, pp 71–82, 2002.

18. S.M. Wiederhorn, “Fracture of Sapphire,” Journal of the American Ceramic Society, Vol. 52, No. 9, pp.485–491, 1969.
19. J.A. Salem, L.J. Ghosn and M.G. Jenkins, “Back-Face Strain as a Method For Monitoring Stable Crack Extension In Ceramics,” *Ceramic Engineering and Science Proceedings*, Vol. 19, No. 3, pp. 587–594, 1998.
20. Private communication by e-mail with William Scott, University of Washington, Seattle, WA, February 11, 2002.
21. B. Asoo, J.M. McNaney, Y. Mitamura, R.O. Ritchie, “Cyclic fatigue-crack Propagation in Sapphire in Air and Simulated Physiological Environments,” J. Biomed Mater Res, 52, pp. 488–491, 2000.
22. Y. Mitamura, and Y. Wang, “Fracture Toughness of Single Crystal Alumina in Air and a Simulated Body Environment,” J. Biomed Mater. Res. 1994; 28: pp. 813–817.
23. M. Iwasa and R.C. Bradt “Fracture Toughness of Single Crystal Alumina,” Structure and Properties of MgO and Al_2O_3 Ceramics, edited by W. D. Kingery, American Ceramic Society, pp. 767–779, 1984.
24. T.A. Michalske, B.C. Bunker and S.W. Freiman, “Stress Corrosion of Ionic and Mixed Ionic/Covalent Solids, “*J. Am. Ceram. Soc*., **69**, 10, pp. 721–724, 1986.
25. S.M. Wiederhorn, “Fracture of Ceramics,” pp. 217–241 in National Bureau Special Publication 303, Proceedings of the conference on Mechanical and Thermal Properties of Ceramics, April 1–2, Gaithersburg, MD, 1968.
26. Private Communication, S.M. Wiederhorn, National Institute of Standards and Technology, Gaithersburg, MD, August 29, 2001.
27. S.M. Wiederhorn, B.J. Hockey and D.E. Roberts, “Effect of Temperature on the Fracture of Sapphire,” Philosophical Magazine, Vol. 28, No. 4, pp. 783–796, 1973.
28. N.J. Petch, J. Congleton, D. Hardie and R.N. Parkins, “Studies of the Brittle Behavior of Ceramic Materials,” Technical Report ASD–TR–61–628, edited by N.M. Parikh, pp. 163, 1964.
29. E.R. Fuller and B.R. Lawn, “Theory for Brittle Flaws Originating from Residual Stress Concentrations,” J. Am. Ceram. Soc. **66**, 5, pp. 314–321, 1983.
30. J.J. Swab, G. Gilde, P.J. Patel A.A. Wereszczak, J. McCauley, and J.D. Risner, “Fracture Analysis of Transparent Armor Ceramics,” Fractography of Glasses and Ceramics IV, Ceramic Transactions, Vol. 122, J.R. Varner and G.D. Quinn, eds., American Ceramic Society, Westerville, OH, pp. 489–508, (2001).
31. Private communication with T.A. Michalske by email, Sandia National Laboratory, Albuquerque, NM, April 10, 2001.
32. Private communication with S.M. Wiederhorn, National Institute of Standards and Technology, Gaithersburg, MD, August 29, 2001, and February 20, 2002.
33. S.S. Smith and B.J. Plekta, “Indentation Fracture of Single Crystal and Polycrystalline Aluminum Oxide,” pp. 189–209 in *Fracture Mechanics of Ceramics*, Vol. 6, R.C. Bradt, A.G. Evans, D.P.H. Hasselman, and F.F. Lange, Eds., Plenum Publishing Co., NY, 1981.
34. W.D. Scott and K.K. Orr, “Rhombohedral Twinning in Alumina,” *J. Am. Cerm. Soc.,* Vol. 66, pp. 27–32, 1983.
35. ASTM C 1161-90, “Standard Test Method for Flexural Strength of Advanced Ceramics at Ambient Temperature,” American Society for Testing and Materials *Annual Book of Standards*, Vol. 15.01, pp. 333–339, 1990.
36. J.A. Salem, N.N. Nemeth, L.M. Powers and S.R. Choi, “Reliability Analysis of Uniaxially Ground Brittle Materials,” *Journal of Engineering for Gas Turbines and Power*, Trans. of the ASME, Vol. 118, pp. 863–871 (1996).
37. J.A. Salem and M. Adams, “The Multiaxial Strength of Tungsten Carbide,” *Ceramic Engineering and Science Proceedings*, Vol. 20, No. 3, pp. 459–466, 1999.

38. Private communication by email with Dan Harris, Naval Warfare Center, China Lake, CA., March 30, 2001.
39. F. Schmid and D.C. Harris, "Effect of Crystal Orientation and Temperature on the Strength of Sapphire," *J. Am. Ceram. Soc*., 81 [4], pp. 885–892, 1998.
40. ASTM C 1499-01 "Determination of Monotonic Biaxial Flexural Strength Advanced Ceramics," pp. 779–788, in Annual Book of ASTM Standards, V. 15.01, American Society for Testing and Materials, West Conshohocken, Pennsylvania (2002).
41. J.A. Salem and L.M. Powers, "Guidelines for the Testing of Plates," pp. 357–364 in Proceedings of the 27th International Cocoa Beach Conference on Advanced Ceramics and Composites: B, *Ceramic Engineering and Science Proceedings*, Vol. 24, No. 4, Waltraud M. Kriven and H.T. Lin, editors (January, 2003).

REPORT DOCUMENTATION PAGE

Form Approved
OMB No. 0704-0188

1. AGENCY USE ONLY (*Leave blank*)	2. REPORT DATE	3. REPORT TYPE AND DATES COVERED
	January 2006	Technical Memorandum

4. TITLE AND SUBTITLE

Slow Crack Growth and Fracture Toughness of Sapphire for the International Space Station Fluids and Combustion Facility

5. FUNDING NUMBERS

WBS 825080.08.02

6. AUTHOR(S)

Jonathan A. Salem

7. PERFORMING ORGANIZATION NAME(S) AND ADDRESS(ES)

National Aeronautics and Space Administration
John H. Glenn Research Center at Lewis Field
Cleveland, Ohio 44135–3191

8. PERFORMING ORGANIZATION REPORT NUMBER

E–15338

9. SPONSORING/MONITORING AGENCY NAME(S) AND ADDRESS(ES)

National Aeronautics and Space Administration
Washington, DC 20546–0001

10. SPONSORING/MONITORING AGENCY REPORT NUMBER

NASA TM—2006-214023

11. SUPPLEMENTARY NOTES

Responsible person, Jonathan A. Salem, organization code RXL, 216–433–3313.

12a. DISTRIBUTION/AVAILABILITY STATEMENT

Unclassified - Unlimited
Subject Category: 27

Available electronically at http://gltrs.grc.nasa.gov

This publication is available from the NASA Center for AeroSpace Information, 301–621–0390.

12b. DISTRIBUTION CODE

13. ABSTRACT ***(Maximum 200 words)***

The fracture toughness, inert flexural strength, and slow crack growth parameters of the *r*- and *a*-planes of sapphire grown by the Heat Exchange Method were measured to qualify sapphire for structural use in the International Space Station. The fracture toughness in dry nitrogen, K_{Ipb}, was 2.31 ± 0.12 MPa$\sqrt{m}$ and 2.47 ± 0.15 MPa$\sqrt{m}$ for the *a*- and *r*-planes, respectively. Fracture toughness measured in water via the operational procedure in ASTM C1421 was significantly lower, K_{Ivb} = 1.95 ± 0.03 MPa$\sqrt{m}$, 1.94 ± 0.07 and 1.77 ± 0.13 MPa$\sqrt{m}$ for the *a*- , *m*- and *r*-planes, respectively. The mean inert flexural strength in dry nitrogen was 1085 ± 127 MPa for the *r*-plane and 1255 ± 547 MPa for the *a*-plane. The power law slow crack growth exponent for testing in water was $n = 21 \pm 4$ for the *r*-plane and $n \geq 31$ for the *a*-plane. The power law slow crack growth coefficient was $A = 2.81 \times 10^{-14}$ m/s·(MPa$\sqrt{m}$)$^{-n}$ for the *r*-plane and $A \cong 2.06 \times 10^{-15}$ m/s·(MPa$\sqrt{m}$)$^{-n}$ for the *a*-plane. The *r*- and *a*-planes of sapphire are relatively susceptible to stress corrosion induced slow crack growth in water. However, failure occurs by competing modes of slow crack growth at long failure times and twinning for short failure time and inert environments. Slow crack growth testing needs to be performed at low failure stress levels and long failure times so that twinning does not affect the results. Some difficulty was encountered in measuring the slow crack growth parameters for the *a*-plane due to a "short" finish (i.e., insufficient material removal for elimination of the damage generated in the early grinding stages). A consistent preparation method that increases the Weibull modulus of sapphire test specimens and components is needed. This would impart higher component reliability, even if higher Weibull modulus is gained at the sacrifice of absolute strength of the component. The current specification frequently used for the preparation of sapphire test specimens and components (e.g., a "60/40" scratch-dig finish) is inadequate to avoid a "short" finish.

14. SUBJECT TERMS	15. NUMBER OF PAGES
Sapphire; Flexural strength; Fracture toughness; Crack propagation; Stress corrosion; Fatigue life; Weibull; Structural reliability; Polishing	52
	16. PRICE CODE

17. SECURITY CLASSIFICATION OF REPORT	18. SECURITY CLASSIFICATION OF THIS PAGE	19. SECURITY CLASSIFICATION OF ABSTRACT	20. LIMITATION OF ABSTRACT
Unclassified	Unclassified	Unclassified	